ISOMORPHOUS FE SUBSTITUTED ZSM-5 FOR METHANE DEHYDROAROMATIZATION

by

Yu-Chieh Cheng

Bachelor of Science, Chemical Engineering, National Tsing Hua University, 2015

Submitted to the Graduate Faculty of

Swanson School of Engineering in partial fulfillment

of the requirements for the degree of

Master of Science

University of Pittsburgh

2017

UNIVERSITY OF PITTSBURGH

SWANSON SCHOOL OF ENGINEERING

This thesis was presented

by

Yu-Chieh Cheng

It was defended on

March 28, 2017

and approved by

Götz Veser, Ph.D., Professor, Department of Chemical and Petroleum Engineering

Giannis Mpourmpakis, Ph.D., Assistant Professor, Department of Chemical and Petroleum Engineering

James R. McKone, Ph.D., Assistant Professor, Department of Chemical and Petroleum Engineering

Thesis Advisor: Götz Veser, Ph.D., Professor, Department of Chemical and Petroleum Engineering

ISOMORPHOUS FE SUBSTITUTED ZSM-5 FOR METHANE DEHYDROAROMATIZATION

Yu-Chieh Cheng, M.S.

University of Pittsburgh, 2017

Shale gas has become an abundant source of natural gas in recent years; methane is one of its major chemical components. Meanwhile, benzene, which is applied into the manufacturing of complex chemicals, is an important chemical intermediate in petrochemical industry. Direct methane dehydroaromatization (DHA) under non-oxidative condition is an alternative approach to convert methane into benzene. The reaction mechanism is generally considered a synergistic result of metal sites and Bronsted acid sites of HZSM-5. Here, methane is activated by metal site while zeolite provides the shape-selective environment and the diffusion channel for reactive molecules. Among different bi-functional catalysts, Mo/HZSM-5 is the most studied catalyst for this reaction due to its strong catalytic performance. However, coke formation driven by thermodynamics will ultimately lead to catalyst deactivation. This problem is exacerbated by the fact that the catalyst regeneration for Mo/ZSM-5 is relatively lengthy and uneconomical due to its loss of activity after burn-off.

Recent reports suggested that atomically dispersed iron on silica can have high conversion of methane to higher hydrocarbon and can potentially suppress coke formation. Our group previously found that highly dispersed iron on ZSM-5, H-(Fe)ZSM-5, also shows high

benzene selectivity and reduced coke formation. However, severe coke formation still result from secondary reactions of product on Bronsted acid site of ZSM-5.

The purpose of this research is to study how catalytic performance and coke formation are influenced by the catalyst structure of H-(Fe)ZSM-5 and how this structure can be affected by the ZSM-5 synthesis. Specifically, the impact of hydrothermal time, hydrolysis time and template ratio in ZSM-5 synthesis were investigated since these parameters can have influence on both crystallinity and particle size. It is found that both of these structural parameters can have significant influence on catalytic performance. In addition, we found that passivation of external Bronsted acid sites can improve catalyst stability by reducing coke formation but simultaneously also decreases the reactivity. Overall, we developed a well-defined catalyst with high selectivity (~86%) in DHA by optimizing only synthetic parameters without applying any post-treatment.

TABLE OF CONTENTS

LIST OF TABLES

LIST OF FIGURES

PREFACE

First, I would like to thank Dr. Götz Veser for his guidance, encouragement and patience over this two years. Thank you for advising me and giving me insight on my research. Without professor, there will be no my success here.

I would like to thank Yahui Yang for helping me solve my research problems and doing most of the characterizations in my research. I believe you will graduate earlier than you expected and find a nice job in United States.

I would also like to thank Yu-Jung Lin for accompanying and guiding me during these years. Without you, I cannot image how do I get through this two years. I hope you become whoever you want to be. All the best.

Particularly, I appreciate that my family is always willing to support me on pursuing master degree abroad.

I am sincerely grateful to everyone who help, support and accompany me over this two years. Thank you all.

1.0 INTRODUCTION

1.1 METHANE DEHYDROAROMATIZATION (DHA)

Shale gas has become an abundant resource of natural gas in United States, which has led to a lower price for methane and renewed interest in converting methane into higher value products. Currently, in the chemical industry, methane utilization proceeds via syngas as an intermediate, which is a highly energy-demanding process. Therefore, direct catalytic conversion of methane into useful products or easily liquefied compounds is an attractive alternative.

Benzene, which is mainly extracted from crude oil, serves as an important chemical feedstock in petrochemical industry. It is primarily used as an elementary petrochemical for manufacturing chemicals with more complicated structure such as cumene, cyclohexane and ethylbenzene. These complicated chemicals can further be used to make plastic essentials comprising polymers, engineering plastics or resins.

Among those catalytic methane conversion, non-oxidative methane dehydroaromatization is a potential way to produce benzene and hydrogen:

$$6CH_{4(g)} \rightarrow C_6H_{6(g)} + 9H_{2(g)}$$

$$\Delta G_r^o = +433\ kJ\ mol^{-1};\ \Delta H_r^o = +531\ kJ\ mol^{-1}$$

Thermodynamic calculations show that this reaction is thermodynamically highly unfavorable.[1] Due to this thermodynamic limitation, the effective activation and conversion of methane is a great challenge. Additionally, benzene formation is minimal at temperature below 600ºC while the formation of solid carbon(coke) is favored above 300ºC. Hence, another challenge for this reaction is the severe coke formation at high temperature, which will further lead to the catalyst deactivation.

1.2 CATALYSTS FOR METHANE DEHYDROAROMATIZATION

ZSM-5 is a crystalline aluminosilicate zeolite, whose framework structure is MFI type with three-dimensional microporous structure. The general chemical formula for ZSM-5 is $M_{x/n}[(AlO_2)_2(SiO_2)_y]\ zH_2O$, where M is an extra-framework cation that neutralizes the anionic charge caused from the charge difference between Al^{3+} and Si^{+4}.[2] M^+, known as cationic exchange site, is widely applied in various types of applications such as waste water treatment/purification and catalytic hydrocarbon conversion. In the case where this cation is in form of proton (H-ZSM-5), a Bronsted acid site (BAS) is formed. More specifically, this Bronsted acid site contains a hydrogen atom bonding to an oxygen atom that is connected to tetrahedrally coordinated cations in ZSM-5 framework.[3] Due to the presence of this acid proton, Bronsted acid sites provide a significant extent of catalytic activity to zeolites, which makes zeolites widely used in petrochemical industry.[4] In addition, uniformly microporous structure with pore diameter ~ 5.6Å in ZSM-5, which is similar to the kinetic diameter of benzene and shown in Fig 1(a), will provide a higher benzene selectivity (shape-selectivity) in DHA reaction. These micropores compose the intersecting microchannel system, which also enable the

molecular transport within ZSM-5 framework, which is shown in Fig. 1(b). Therefore, these unique properties make ZSM-5 an extensively studied catalyst for DHA reaction.

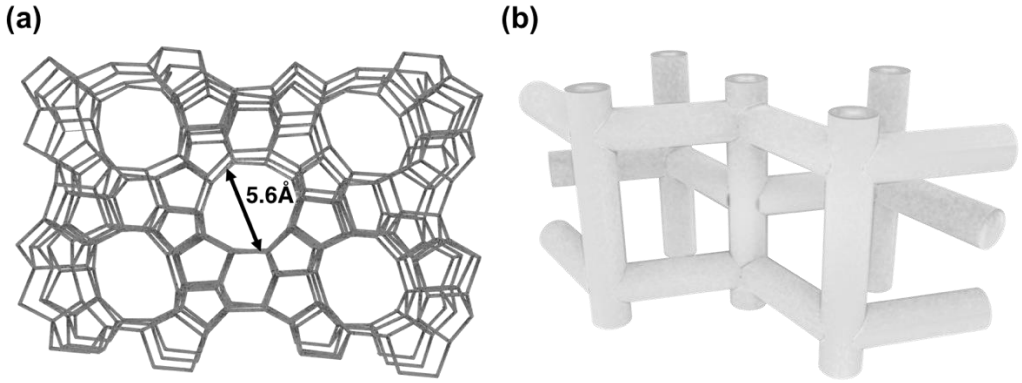

Fig. 1 ZSM-5 framework: (a) microporous structure with pore diameter around 5.6Å (b) Intersecting microchannel system.

Methane is one of the most stable organic molecule due to its strong C-H covalent bond which has bond energy ~ 435kJ/mol. Therefore, the efficient activation and direct conversion of CH_4 to higher hydrocarbons is an inevitable challenge in catalysis. Since ZSM-5 does not possess the ability to activate methane, an additional catalytic component is required to catalyze methane activation.[5] ZSM-5 doped with transition metals such as Mo, Cu, Zn, and Cr, serve as bi-functional catalysts, which are active for DHA and are demonstrated to provide high selectivity for benzene.[6–8] The general mechanism is that methane is dehydrogenated on transition metal site, and forms C_2H_X intermediate which further undergoes aromatization at Bronsted acid site of ZSM-5, which is shown in Fig. 2. By far the most intensively studied bi-functional catalyst for DHA reaction is Mo/HZSM-5 due to its high activity (conversion, ~10%[1])

and aromatic selectivity (benzene selectivity, 60~80%) at 700ºC reaction temperature. However, the catalyst deactivation problem at high reaction temperature is still an inevitable challenge.

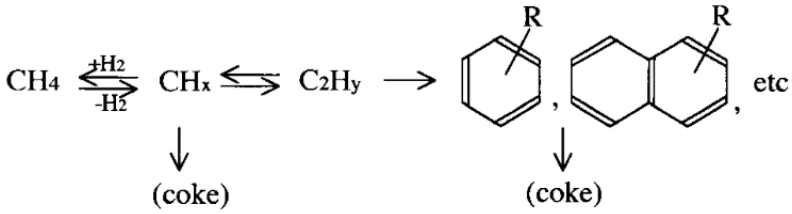

Fig. 2 Illustrative mechanism for formation of aromatics and coke in methane dehydroaromatization from Ohnishi et al.[9]

1.3 ISSUES ASSOCIATED WITH CURRENT CATALYSTS

The formation of solid carbon causing catalyst deactivation and the thermodynamic limitations resulting in low methane conversion are the two major issues in DHA reaction.

Even for the currently best bi-functional catalyst, Mo/HZSM-5, poor stability due to catalyst deactivation is still a major problem, especially at high temperature. For catalytic reactions, micropores in ZSM-5 provide shape product selectivity and are used as a molecular transportation channel which allows molecules to diffuse inside the structure. Nonetheless, the small micropores result in slow transport of hydrocarbon inside these micro-channels, which will lead to secondary reaction with BAS and formation of carbonaceous residues (coke). This coking deactivates the catalyst either by covering the active site or blocking micro-channels within its structure.[10,11]

The kinetic limitation in this endothermic reaction can be relieved by doping transition metals onto the zeolite to decrease the activation barrier, while the thermodynamic limitations can be countered by increasing the reaction temperature to drive equilibrium towards products, which is shown in Fig. 3(a). However, while at high temperature thermodynamics favors conversion of methane to benzene, it also drives equilibrium to more coke formation and significantly reduce the benzene selectivity, which is shown in Fig. 3(b). Therefore, from these thermodynamics analysis using HSC 7.1 software, the mostly studied temperature is 700 ^{0}C.[12]

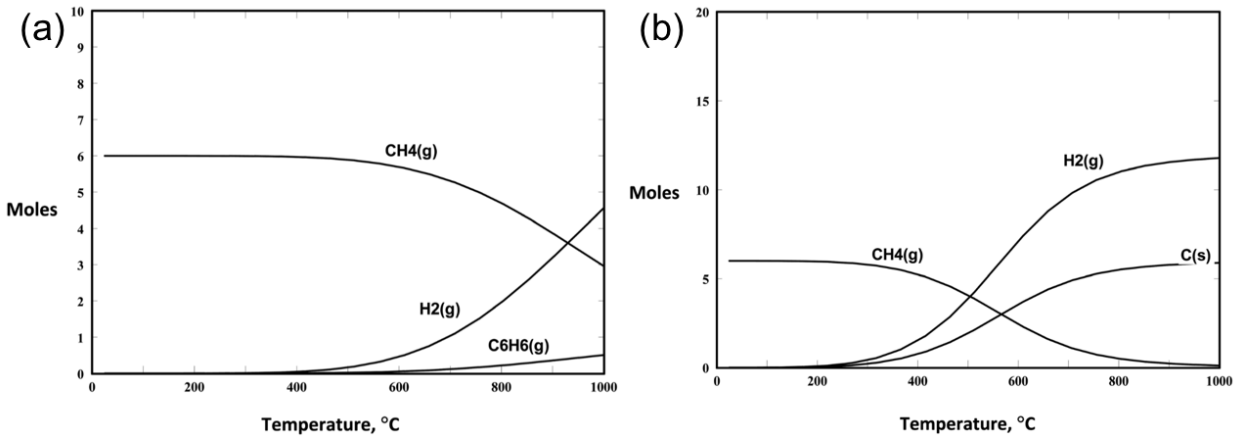

Fig. 3 Calculation of equilibrium amount(moles) under 1 bar from Spivey et al., starting from 6 mol of CH_4 and involving (a) H_2 and C_6H_6 as products (b) $C_{(s)}$, H_2 and $C_6H_{6(g)}$ as products.[1]

1.4 APPROACHES FOR IMPROVING DHA REACTION

Many efforts have been contributed to optimization of DHA reactions either by catalyst or reactor design to enhance methane conversion, benzene selectivity and catalyst life time.

1.4.1 Zeolite

A wide range of zeolites has been investigated as catalysts for DHA reaction. Among these candidates, ZSM-5 and MCM-22 are extensively studied due to their high selectivity towards benzene. In comparison of ZSM-5 and MCM-22, Bai et al. concluded that Mo/MCM-22 can have a longer catalyst lifetime (stability) and higher benzene selectivity since, in addition to small pores, MCM-22 has relatively large 12-membered ring cages to alleviate diffusion limitation and further resist coke formation (with dimension of 1.8 x 0.71 x 0.71 nm).[13] Nonetheless, the circular channels and larger pore mouth structures of ZSM-5 will result in a better dispersion of Mo, and hence the methane dimerization rate coefficient ($2CH_4 \rightarrow C_2H_4 + H_2$) is much greater than Mo/MCM-22. Therefore, in this thesis, ZSM-5 as a support is the only studied case for DHA.

1.4.1.1 Hierarchical-Zeolite-Based Catalyst for DHA

Zeolites possess a well-defined hydrothermally stable framework with uniformly microporous structure which contribute to the shape selectivity and diffusion pathway. Nonetheless, microporous channel structure can also be one of major drawback for zeolites utilizing in catalytic reaction since the molecules transportation is limited through pores with molecular dimensions. This dilemma will enhance the chance of hydrocarbon undergoing secondary reaction and finally cause catalyst deactivation.

One of possible solutions is the development of mesopores (2 nm< d_p < 50 nm) in ordered microporous materials.[14,15] This type of material consists of different porosity scales, which is

called hierarchical porous materials. While micropores in zeolites provides active site and shape-selectivity, mesopores will facilitate transportation of molecules within zeolites framework. Chu et al. developed a hierarchical Mo/HZSM-5 containing mesopores which showed an improvement in both activity and stability in DHA reaction. In their case, mesopores are formed within an aggregate crystal which has intercrystalline voids between the French fries-like crystals instead of pores inside a single crystal.[15]

Generation of mesopores inside crystalline zeolites can be achieved via post-synthesis treatment which is typically done by top-down method. Hydrothermal treatment, acid leaching and alkali-treatment are typical post-synthesis treatment to introduce mesopores in zoelites. Mesoporous zeolite synthesized via dealumination treatment[16] or desilication[17,18] are well studied in recent years. One of the major drawbacks of dealumination treatment is the impact on acidity of zeolite due to the dislodgement of Al in framework. Also, for high siliceous zeolites (high Si to Al ratio), the development of mesoporosity via dealumination is limited due to minority of Al. On the other hand, desilication is shown to be a promising method for developing mesopores.[19] Comparing to dealumination, one feature of desilication by alkaline treatment is the preservation of Bronsted acid site, which means it has no significant influence on acidity of zeolite.

An alternative approach for developing mesoporosity of zeolite is templating method, which is done by bottom-up method. Various types of template such as supramolecular and carbon templates are applied to the formation of mesopores during zeolite crystallization. By far, carbon templating is the most investigated, which the results can be versatile due to the various types of carbon used. Taking carbon black templating for example, Jacobsen et al. found that using excess zeolite gel can encapsulate carbon particles, and removal of carbon particles by burn-off will result in uniform mesopores within zeolite crystal.[20] The same group also

demonstrated that multi-wall carbon nanotube templating can generate straightly worm-like channels through the entire zeolites.[21] Therefore, by properly choosing the carbon particles or tailoring the width of nanotube, it is possible to develop different size of mesopores in zeolite crystal. Other than synthesizing mesoporous zeolites, carbon templating can also be used to yield nanosized zeolite crystals, which will be discuss in the next chapter.

1.4.1.2 Nanocrystalline Zeolites

Nanocrystalline zeolites have started gaining interests due to their intriguing properties such as higher surface area and reduced diffusion path lengths, compared to micro-sized zeolites.

As zeolites crystal size is scaled down to nanoscale, the external surface area becomes distinct, which is originally negligible in microsized zeolites. When more active sites are located on the external surface, the catalytic activity of zeolite crystal can be enhanced since more Bronsted acid site will directly expose to reactant.[22,23] In addition, a smaller particle size can result in a shorter diffusion pathway within ZSM-5 structure. The reduced diffusion path lengths of nanocrystalline zeolites, comparing to micron-sized zeolites, can result in a decreased chance of products undergoing secondary reaction through micro-channels inside zeolites, which means coke formation can be resisted.

However, shape selectivity, one of the most important benefits from micropores in zeolites, is diminished because the volume of micropores is reduced within individual zeolite crystal, if the crystal size is scaled down to nanosized crystal.[24] Furthermore, higher reactivity on the external surface can facilitate coke formation deposited on the external surface, which may cover the pore mouth of micro-channels, lead to a faster catalyst deactivation and lower product selectivity.

Although there is extensive literature studying catalytic properties of nanocrystalline zeolites, nanocrystalline zeolite is rarely applied into DHA reaction.[24,25] Yanbin et al. studied the catalytic performance of nanocrystalline Mo/ZSM-5 synthesized via ball-milling method.[25] However, the results are not only affected by various crystal size but also by the changes in acidity due to the destruction of ZSM-5 framework by top-down method.

1.4.2 Metal sites

It is well known that methane is a stable organic molecule due to its strong C-H covalent bond ($\Delta_d H$ = 440kJ mol^{-1}). Accordingly, an additional catalytic material is required to catalyze methane since zeolite itself is unable to activate methane. Wang et al. first reported that transition metal ions can serve as the active site for activating CH_4 in methane dehydroaromatization under the condition of non-oxidation.[26] Importantly, the transition metal may be stabilized via migration into the framework of zeolites which also form a bi-functional catalyst with intriguing catalytic properties.[27] . Since then, several types of transition metal modified zeolites were evaluated so as to improve the catalytic activity, product selectivity and catalyst stability. Xu et al. and Lunsford et al. investigated the catalytic performance of various transition metals deposited on ZSM-5; the results are shown in Table 1.[6–8] Among these transition metal ion modified ZSM-5, Mo/ZSM-5 has the best catalytic performance on either CH_4 conversion or aromatic selectivity. Currently, Re/HZSM-5 is only catalyst that catalytic activity is comparable to Mo/ZSM-5.[28] However, due to the high cost of Re, Re/HZSM-5 is not widely studied.

Most metal loaded zeolites for catalysis are made by impregnation method, ion-exchange method or vapor phase deposition.[29] From results reported by Lunsford et al., even though the

same metal are loaded on zeolites, it can have different catalytic performance due to the different synthesis method. Taking Mo/ZSM-5 for an example, a catalyst synthesized by impregnation method can show as much as 7.6% methane conversion while a catalyst made by solid state ion-exchange shows only 2.6% conversion.[7] This variation can be attributed to the difference in catalyst structure and material properties resulted from different synthesis method. However, most of reported catalyst are not only made by various synthesis method but also under different reaction conditions. Accordingly, a systematic investigation is still required for the study of metal site in DHA.

Table 1 Catalytic performance on DHA of various transition metal ion loaded ZSM-5 from ref. [6] and [8].

Transition metal ion	Preparation Method	Temp. [K]	Space velocity [ml/g h.]	Conv. of CH_4 [%]	Select. To aromatics [%]	Reference
Zn	Impregnation	973	1500	1.0	79.1	6
Cu				0.6	52.5	
Pt				0.03	0	
Ni				0.01	0	
Mo		1023	800	7.6	78.4	8
Fe				4.1	61.8	
V				0.6	63.1	
Cr				0.3	19.4	
W				0.7	0	

2.0 OBJECTIVES

Mo/ZSM-5 is the most widely studied bi-functional catalyst for DHA reaction and exhibits the best catalytic performance, making DHA a potential route to produce benzene. However, catalyst deactivation and lengthy regeneration cycles[12] make DHA over Mo/ZSM-5 difficult to apply on an industrial scale due to the economic viability. While majority of literature primarily focus on Mo/ZSM-5, the issues mentioned above encourage our investigations of other potential catalyst candidates which are active and stable for DHA reaction.

Previously, our group reported that highly dispersed Fe modified ZSM-5 via isomorphous substitution, H-(Fe)ZSM-5, can have a great benzene selectivity (~60%) and can suppress coke formation from metal site. Nonetheless, the reached maximum CH_4 conversion is still poor (~1%), and the coking generated from secondary reaction of product still lead to a catalyst deactivation. In this work, we aimed to improve the catalytic performance of H-(Fe)ZSM-5 and reduce coke formation via controlling zeolite particle size. As discussed above, a shorter diffusion pathway for molecule transportation can potentially enhance the catalytic performance and simultaneously reduce the chance for product undergoing secondary reaction. To investigate the particle size effect on catalytic performance, control over particle size was achieved by modifying synthetic parameters such as hydrothermal time and template/silica ratio. Therefore, the ultimate objective of this research was to develop a well-defined and particle-size controllable H-(Fe)ZSM-5 catalyst with improved activity, high benzene selectivity and long-

term catalyst stability in DHA reaction. Working towards this goal, we aimed to inspect systematically how the catalytic performance and coke formation are influenced by the changes in material properties.

3.0 ISOMORPHOUS FE SUBSTITUTED ZSM-5

Iron, the fourth most common element in the earth, has started gaining attention as a potential DHA catalyst due to its low cost and low toxicity. Bao et al. demonstrated that iron-silica catalyst can be a compelling catalyst for catalytic conversion of methane to ethylene and aromatics at high temperature (1363K), with methane conversion reaching a maximum at 48.1%.[30] More intriguingly, they reported that the lattice-confined single iron sites (isomorphous substituted iron) provide stable catalytic performance, which suggests that this atomic dispersed Fe can effectively suppress coke formation. The catalytic activity results are shown in Fig. 4.

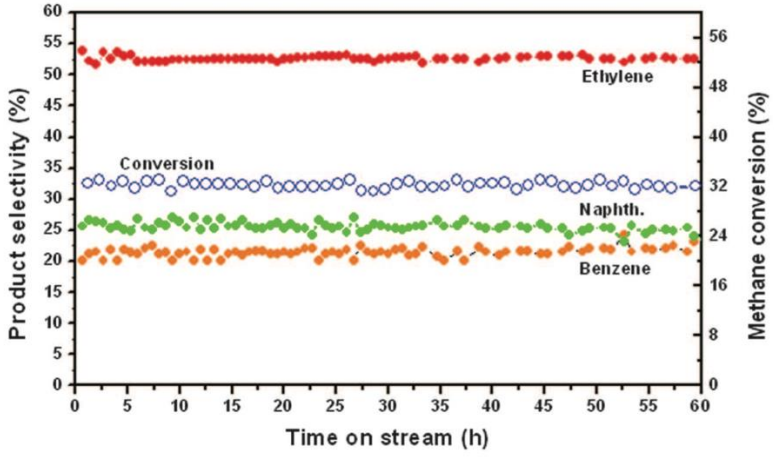

Fig. 4 Reactivity results from X. Guo's group: a long-term catalyst stability test of 0.5%Fe©SiO_2 at 1293K and 14.5 liter $gcat^{-1}$ h^{-1}.[30]

Recently, our group studied the nature of active species in Fe-containing ZSM-5 and the catalytic performance on DHA reaction.[31] Different from other Fe-HZSM-5 prepared via either ion-exchanged or core-shell synthesis, isomorphous Fe substituted ZSM-5 delivers a higher benzene selectivity, which is presented in Fig. 5(a). Moreover, the results in fig. 5(b) and (c) confirmed that coke formation is diminished with increasing of Fe dispersion, although the presence of Bronsted acid sites still causes coke formation via secondary reaction of aromatic product inside microporous structure of ZSM-5. The possible secondary reaction of aromatic product may involve olefin polymerization, formation of polynuclear aromatics from benzene and olefin cyclization from substituted benzenes.[11]

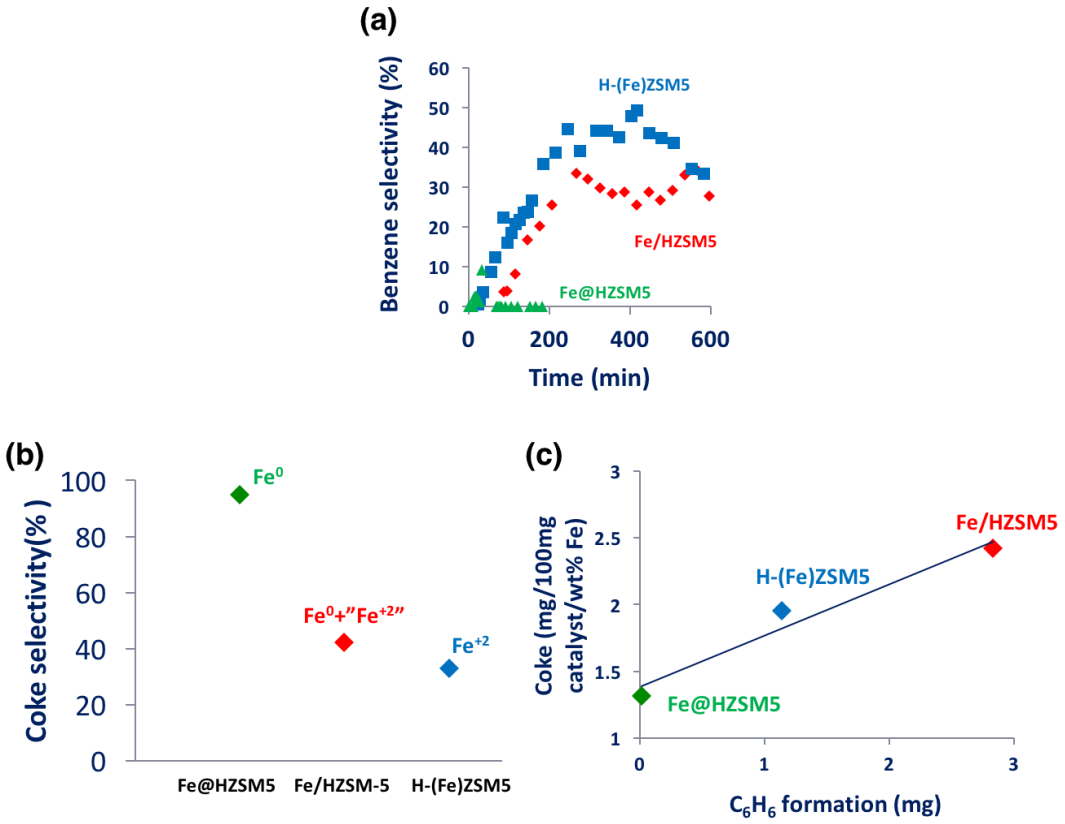

Fig. 5 Reactivity results of coreshell structure, atomic dispersed and ion exchanged Fe-HZSM-5 from Y. Lai's group: (a) C_6H_6 selectivity, (b) coke selectivity including the oxidation state of Fe and (c) coke amount vs. benzene formation. H-(Fe)ZSM-5, Fe/HZSM-5 and Fe@HZSM-5 refer to isomorphous Fe substituted ZSM-5, ion exchanged Fe-ZSM-5 and Coreshell Fe-ZSM-5.[31]

By understanding the potential of this isomorphous Fe substituted ZSM-5 (H-(Fe)ZSM-5), we aim to optimize the catalytic performance of H-(Fe)ZSM-5 via tuning its crystal size. There are several routes to affect particle size of zeolites such as ball-milling[25], modifying synthetic parameters and templated synthesis. Top-down method is not considered as an option in this study since it may cause side effects such as structural destruction which leads to poor crystallinity. Templated methods are often expensive, environmentally unfriendly, and need

additional treatment to remove the template. Moreover, the removal of template via calcination can result in aggregation of nanocrystalline zeolites.[32] Therefore, in this study, we investigate how to control ZSM-5 crystal size via modifying synthetic parameters in order to study how catalytic performance is affected by ZSM-5 crystal size.

3.1 EXPERIMENTAL

3.1.1 Material synthesis

H-(Fe)ZSM-5 (Isomorphous substitution). H-(Fe)ZSM-5 was synthesized by an isomorphous substitution route.[33] Typically, an aqueous solution of $Fe(NO_3)_3$ (99.99%, Sigma Aldrich) was first prepared. 0.033 moles of Tetraethoxysilane (TEOS) was added dropwise to the above mixture and stirred for 3 h. Then, NaOH was added into a premade mixture of structure directing agent (SDA), Tetrapropylammonium Hydroxide (TPAOH, 20 wt % in aqueous solution), and $Al(NO_3)_3$ (>98%, Sigma Aldrich). TEOS solution with Fe precursor was then added dropwise into TPAOH solution, and formed opaque solution with calculated molar ratios between the components as H_2O/Si=45, TPAOH/Si=0.1, NaOH/Si=0.2, Si/Al=125, and Si/Fe=152. The solution was then sealed in a Teflon-lined stainless steel autoclave and transferred into hydrothermal reactor for hydrothermal treatment at 175°C for 5 days. The product (Na-(Fe)ZSM-5) was washed with deionized (DI) water and dried at 100°C, followed by calcination at 550°C in air for 5 h. Next, Na-(Fe)ZSM-5 was converted to H-(Fe)ZSM-5 by ion exchange with aqueous NH_4NO_3 solution (1M) at 80°C for 12 h. Finally, the material was dried at 100°C in vacuum and calcined at 500°C in air for 5 h. The synthesis procedure is shown in Fig. 6.

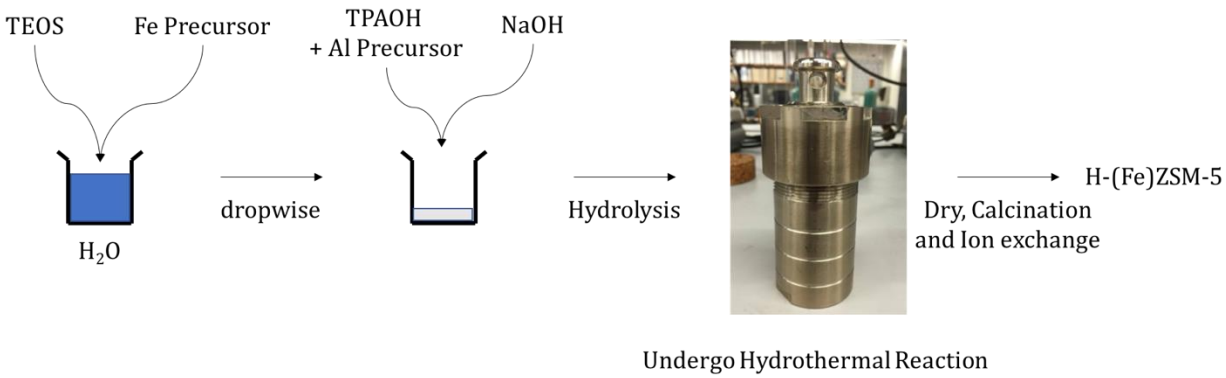

Fig. 6 General synthesis method for H-(Fe)ZSM-5

3.1.2 Catalyst characterization

X-ray diffraction (XRD). Powder X-ray diffraction (XRD) measurements were performed with a high-resolution powder X-ray diffractometer (Bruker D8 Discover) using monochromatic CuKα radiation at the wavelength of 1.54 Å. The beam voltage was 40 kV at a current of 40 mA.

The diffraction patterns were recorded with a step of 0.02º(2θ), 0.5 sec/step. Relative crystallinity was measured using Integrated Peak Area method established by ASTM.[34] The baseline was constructed from the center of the background scatter at 22º 2θ to the center of background scatter at 25.0º 2θ on the XRD pattern. The integrated peak areas of each spectrum were calculated from 22º 2θ to 25º 2θ. The calculation formula is shown below, and demonstrative XRD pattern is shown in Fig. 7.

$$\%\ XRD\ relative\ crystallinity\ ZSM\text{-}5 = \frac{S_s}{S_r} \times 100$$

Where:

S_s = Integrated peak area for the sample, and

S_r = Integrated peak area for the reference.

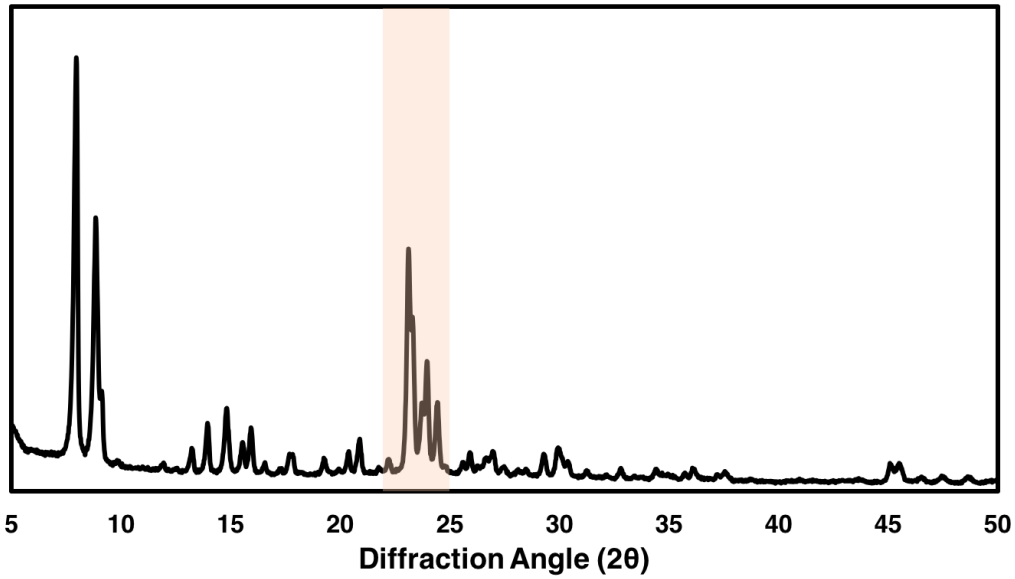

Fig. 7 Demonstrative XRD pattern of H-(Fe)ZSM-5. The integrated peak area was calculated from 22º 2θ to 25º 2θ which is illustrated in orange area.

Electron microscopy and X-ray microanalysis. A JEOL JSM-6510LV field emission scanning electron microscope (SEM) was used to determine material morphology at beam voltage of 20 kV. Samples were dispersed on carbon type support and were sputter coated with a thin palladium film prior to characterization. Nanoscale morphology was determined by a high-resolution transmission electron microscopy (HRTEM, JEOL-2100). Samples were dispersed on a copper type-B support grid (Ted Pella Inc.).

Surface area and porosity analysis. Surface area and porosity were determined via nitrogen sorption in a Micromeritics ASAP 2020. Samples were degassed for 24 hours at 300 °C under high vacuum prior to each analysis. Both nitrogen adsorption/desorption measurements were performed at liquid nitrogen temperature (77 K), which is illustrative in Fig. 8(a). The typical test involved a 6-point Brunauer- Emmett-Teller (BET) analysis for total surface area measurement in the relative pressure range $0.1<P/P_0<0.35$. Mesopore size, volume, and surface area determination were calculated by the Barret-Joyner-Halenda (BJH) adsorption diagram which is shown in Fig. 8(b). All reported pore properties were acquired by analyzing the adsorption isotherm data.

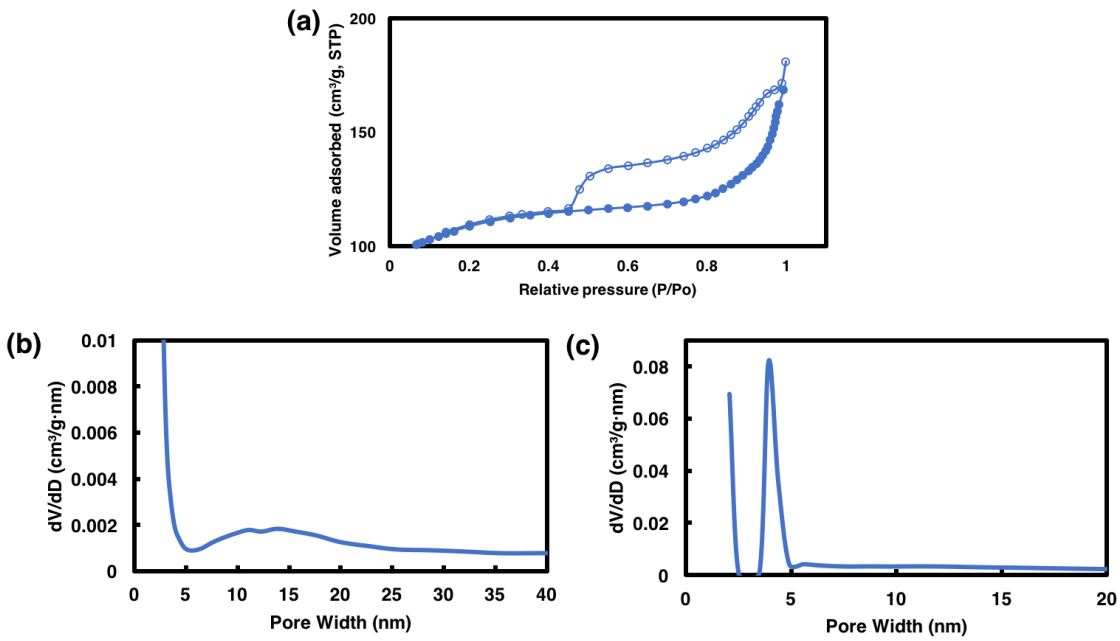

Fig. 8 Demonstrative porosity analysis of H-(Fe)ZSM-5: (a)N_2 adsorption/desorption isotherm, (b)BJH adsorption diagram and (c)BJH desorption diagram. BET analysis was measuring from $P/P_o = 0.1$ to $P/P_o = 0.35$. Mesopore volume was calculated using BJH adsorption diagram.

3.1.3 Reactivity evaluation

The reaction was carried out in a fixed-bed reactor at 700ºC and atmospheric pressure. Typically, catalysts were charged into a 5.0 mm i.d. quartz tubular reactor. The reactor tube was heated from room temperature up to 500ºC for catalyst pretreatment in air, and then heated to desired reaction temperature (700ºC) under helium flow. After temperature equilibration, methane (6.25 sccm) was introduced onto the catalyst. The typically used gas hourly space velocity (GHSV) was 3750 (cc/g/hr) for catalytic performance comparison between different catalysts. The effluent gas products were analyzed by both Balzers Quadstar GSD 300 mass spectrometer (MS) and Agilent 3000A Micro GC equipped with thermal conductivity detectors (TCD). An amount of 50% He was added to the methane feed as an internal standard. The methane conversion and selectivity of products was evaluated according to the carbon mass balance. The equations used to calculate conversion, selectivity and yield are shown below. Each the catalyst was evaluated at least twice to assure the reproducibility of reactivity data. The results were within ±3.5% error. Carbon balance were calculated using equations below. Carbon balance error were within 5%.

$$Methane\ conversion:$$

$$X_{CH_4}[\%] = \frac{molar\ flowrate\ of\ CH_{4_{in}} - molar\ flowrate\ of\ CH_{4_{out}}}{molar\ flowrate\ of\ CH_{4_{in}}} \times 100$$

$$molar\ flowrate\ of\ CH_4 = volumetric\ flowrate \times concenration\ of\ CH_4$$

$$volumetric\ flowrate_{out} = volumetric\ flowrate_{in} \times \frac{concenration\ of\ He_{in}}{concenration\ of\ He_{out}}$$

$$Benzene\ selectivity:$$

$$S_{C_6H_6}[\%] = \frac{volumetric\ flowrate_{out} \times concentration\ of\ C_6H_6}{molar\ flowrate\ of\ CH_{4_{in}} - molar\ flowrate\ of\ CH_{4_{out}}} \times 6 \times 100$$

$$Benzene\ yield:$$

$$Y_{C_6H_6}[\%] = \frac{X_{CH_4} \times S_{C_6H_6}}{100}$$

Carbon Balance error:

$$Error_{carbon\ balance}\ [\%]$$

$$= \frac{volumetric\ flowrate_{carbon,in} - volumetric\ flowrate_{carbon,out}}{volumetric\ flowrate_{carbon,in}} \times 100$$

$$volumetirc\ flowrate_{carbon,in} = volumetric\ flowrate_{CH_4,in}$$

$$volumetirc\ flowrate_{carbon,out}$$

$$= volumetric\ flowrate_{CH_4,out} + volumetric\ flowrate_{C_2H_4,out}$$

$$+ volumetric\ flowrate_{C_2H_6,out} + volumetric\ flowrate_{C_6H_6,out}$$

$$+ volumetric\ flowrate_{CO_2,out} + volumetric\ flowrate_{CO,out}$$

3.2 CONTROL OF CRYTALLINITY AND PARTICLE SIZE VIA VARYING HYDROTHERMAL TIME

In zeolite synthesis, hydrothermal reaction often serves as a crucial crystallization step for amorphous silica. When zeolite start crystallization in hydrothermal reaction, amorphous silica will be gradually converted into zeolite, and crystallinity will be enhanced. In addition, hydrothermal reaction will also crystal growth due to the presence of dissolved precursor in synthesis solution. For example, Van Grieken and coworkers reported that with longer hydrothermal time, zeolite with bigger particle size and better crystallinity can be achieved, although crystallinity should reach a completed crystallization at a certain duration.[35]

Most zeolites synthesis for catalysis reaction use a very long hydrothermal time (120h) to ensure the completely crystallization due the requirement of well-defined structure. However, indeed, crystallization do not require that lengthy time duration to reach the maximum crystallinity. The proper choice of hydrothermal time can significantly reduce the synthesis cost resulting from high temperature requirement. Furthermore, from catalysis perspective, crystal growth and enhancement of crystallinity can be considered as counter factors. A bigger particle size will lead to unselective reaction due to a greater chance for secondary reaction and a faster catalyst deactivation, whereas improved crystallinity will favor selective reaction due to the well-defined structure. Hence, one of our goals is to study how these factors affect catalytic performance and choose a proper hydrothermal time for further investigations. In addition, the synthesis mixture before hydrothermal reaction in this study is opaque solution which implies there are precipitated particles formed already, whereas the synthesis mixture before hydrothermal reaction in most of literature are in form of supersaturated hydrogel. This indicates

that results from Van Grieken et al. cannot directly be applied into our case. Therefore, in this study, another goal is to inspect the crystallization mechanism within this system.

3.2.1 Results and Discussion

3.2.1.1 Material characterization

As mentioned above, with a longer hydrothermal time, ZSM-5 with a bigger particle size and a better crystallinity can be obtained. However, in catalytic perspective, these two factors can result in opposite effects, which a bigger particle size will lead to a greater chance for product undergoing secondary reaction while a better crystallinity can provide shape-selectivity to reactions. To find the sweet spot of these two counter factors and investigate crystallization mechanism from our synthesis system, a systematic investigation was carried out with varying the hydrothermal time at 175ºC. Taking reference from Van Grieken et al., ZSM-5 with 0h, 6h, 12h, 18h, 24h, 48h and 120h hydrothermal treatment were synthesized to investigate the change of both crystallinity and crystal size.

Fig. 9(a) shows that before hydrothermal reaction, there are particles formed already, and most particles were below 300 nm while some particles are extremely large, which are around 10-70μm, which is shown in Appendix A. After 6h of hydrothermal reaction, the absence of those extremely large particles probably indicates that they were split into smaller particles, and some bigger particles(~3μm) are formed. At 12h, most of particles grow up to 3μm - 4 μm and crystalline facet started appearing on morphology. Intriguingly, after 18h, we start to observe that parts of zeolite particles begin to decrease their average size, which is shown in Fig. 11. Moreover, the dramatic decrease of particle size between 18h and 24h is not quite understood

yet. The specific cause for these decreasing of average particle size still need a further investigation. Above 24h, the majority of size of zeolite particles is close to 1 μm. For hydrothermal time above 24h, particle size started to grow smoothly. However, interestingly, it is found that as hydrothermal time increase up to 120h, it seems to have two different size of particles which one is much larger than another one. In this case, Ostwald ripening is a likely explanation for this phenomenon. Smaller particles would dissolve and redeposit onto surface of larger particles which will eventually lead to two different type of particle sizes.

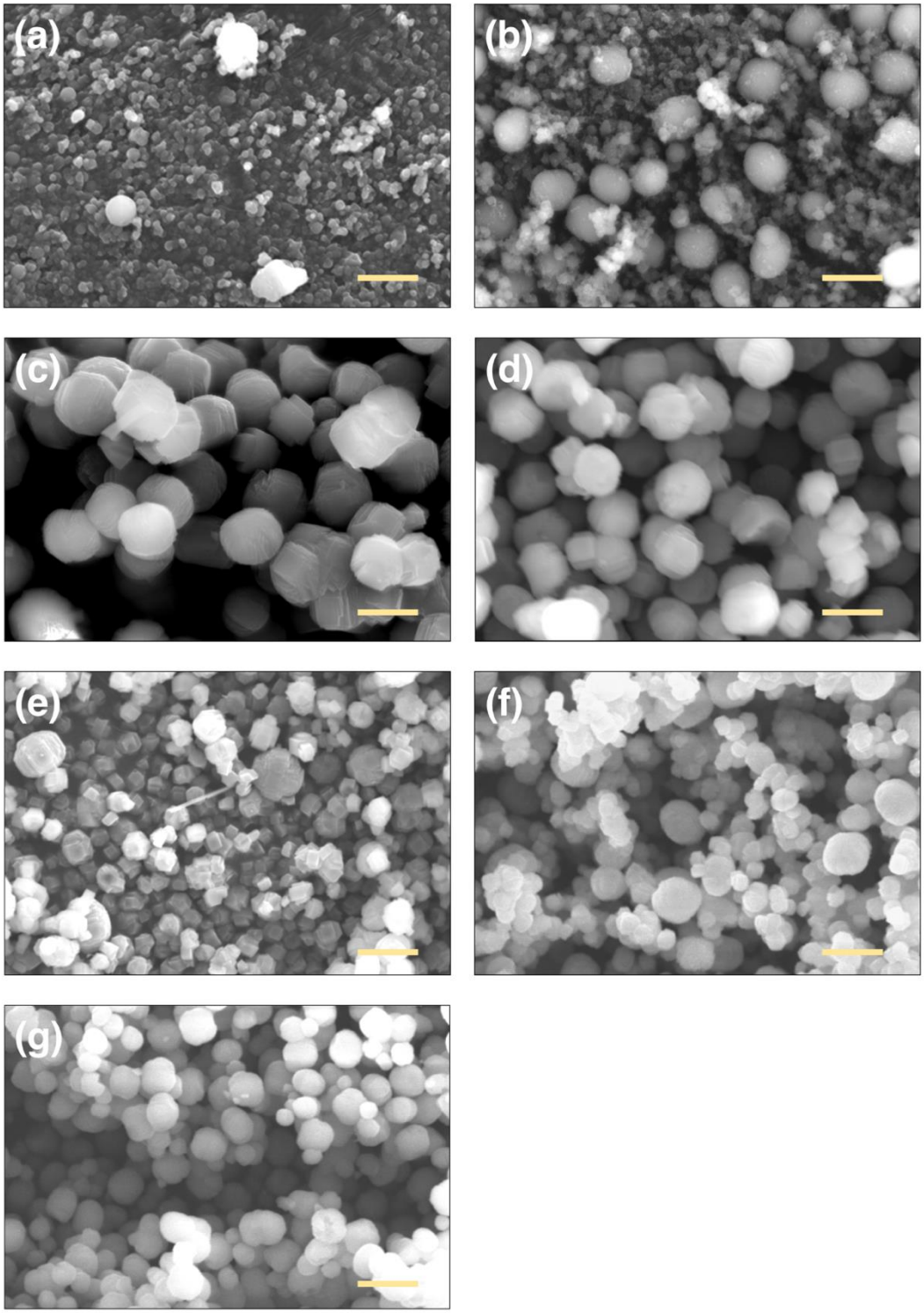

Fig. 9 Scanning electron microscope images of different hydrothermal time: (a) 0h, (b) 6h, (c) 12h, (d) 18h, (e) 24h, (f) 48h and (g) 120h. All the scale bars are 5μm.

Fig. 10 presents the XRD pattern of as-synthesiszed H-(Fe)ZSM-5 samples with different hydrothermal times. As expected, it shows that the shorter hydrothermal time exhibits poorer crystallinity. Before undergoing hydrothermal reaction, the solid materials are confirmed as completely amorphous silica (bottom curve). After 6h hydrothermal treatment, it starts to show the crystalline peaks of MFI structure with some remaining broad amorphous silica peaks. Then, the broad amorphous silica peak disappeared after 12h hydrothermal treatment while above 24h hydrothermal treatment, crystallinity have achieved a value close to complete crystallization which the relative crystallinity value is shown in Fig. 11. The reference spectrum is taken from 120h sample, and the slightly lower relative crystallinity of 48h sample is possibly due to the measurement error.

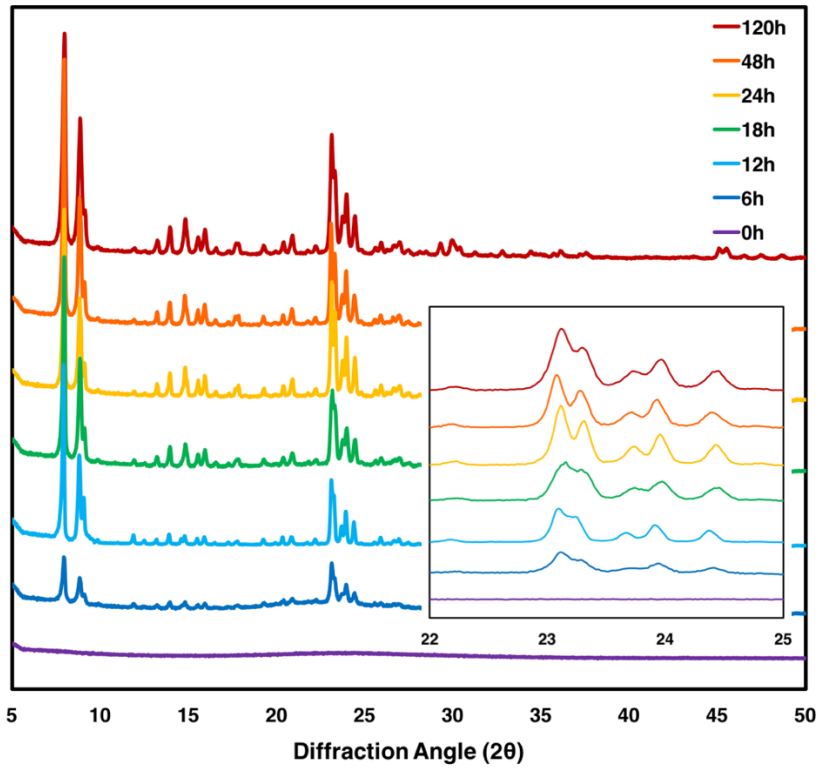

Fig. 10 XRD spectrum of as-synthesized samples obtained at various hydrothermal time.

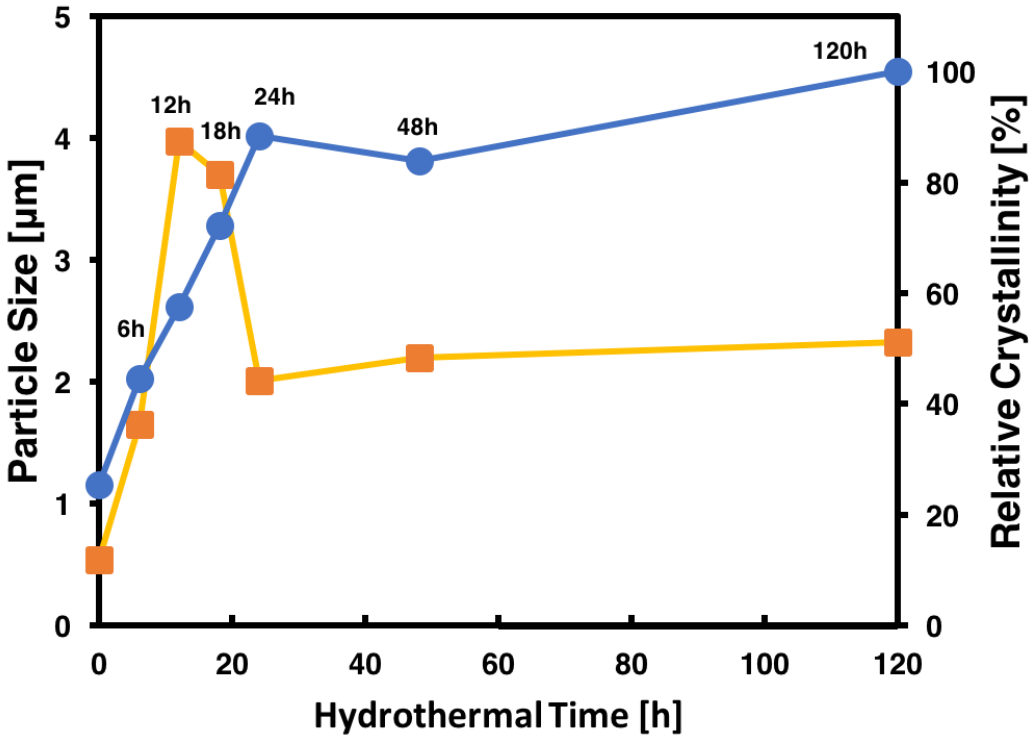

Fig. 11 Correlation between average particle size/relative crystallinity and hydrothermal time. The right y-axis refers to relative crystallinity calculated from Peak height method. The left y-axis refers to average particle size.

3.2.1.2 Catalytic performance

To study the dependences of catalytic performance on particle size and crystallinity, catalytic evaluation of three samples with different hydrothermal time treatment was conducted. Based on the crystallinity in Fig. 10, a transition from insufficient crystallinity to fully crystallized occurs between 18h and 24h, and 48h hydrothermal treatment sample possess a slightly larger particle size and similar crystallinity with 24h hydrothermal treatment. Therefore, by choosing these three sample for catalytic evaluations, the influence of crystallinity and particle size on catalytic

performance should be able to be observed. Fig. 12 presents the reactivity results of DHA reaction from 18h, 24h and 48h hydrothermal treatment samples. For Fig. 12(a), the relatively poor methane conversion from sample with 18h hydrothermal treatment can be attributed into its lack of crystallinity and large crystal size. The samples with 24h and 48h hydrothermal treatment have relatively similar crystal size and crystallinity which result in a similar maximum value of methane conversion. Although there is no dramatic particle size difference between 24h and 48h, a lightly smaller crystal size of 24h sample, which is shown in Fig. 11, may result in a longer time for achieving maximum methane conversion. This implies that induction period is longer, which means the transformation rate of catalyst from ordinary phase to active phase is slower. Nonetheless, the detailed cause for this change still needs a further investigation. For Fig. 12(b), it is found that with sample with 24h hydrothermal treatment has a greater selectivity, presumably due to its relatively smaller particle size and higher crystallinity, comparing to the other two samples. The consequence on catalytic performance of this difference in crystal size can be observed more clearly in either Fig. 12(c) or (d), which shows that a smaller particle can have more benzene productions or benzene yields.

The correlations of crystallinity and crystal size with catalytic reactivity confirm that a well-defined crystal structure is required for a good catalyst, which means crystallinity has more pronounced effect on reactivity than particle size.

As discussed above, one of the purpose for this chapter is to find a sweet spot for these two factors to have a basis for further investigations. Therefore, H-(Fe)ZSM-5 with 24h hydrothermal treatment will be set as the basis for further studying in next chapters.

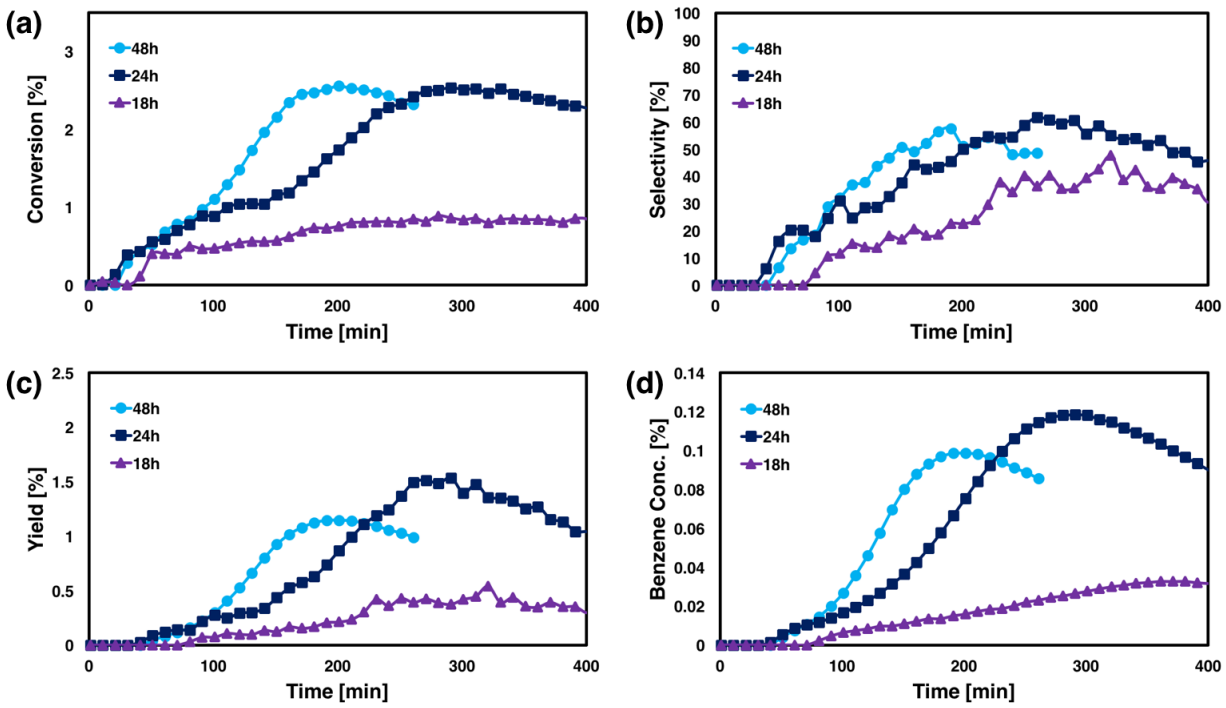

Fig. 12 Reactivity data for H-(Fe)ZSM-5 catalysts with different hydrothermal time at 700ºC: (a) Methane conversion, (b) Benzene selectivity, (c) Benzene yield and (d) Benzene conc.. GHSV: 3750 cc/g/h (50%CH_4 and 50% He)

3.2.2 Conclusion

Overall, the growth trend of ZSM-5 crystal does not follow the previously reported results of by Van Grieken and coworkers, possibly due to the difference in synthesis system. The starting mixture in our synthesis system is in form of opaque solution which means visible particles formed already, while their case is in transparent gel which has no solid particle formed yet. SEM images shows the unusual trend of growing-shrinking-growing mechanism. Nonetheless, the detailed cause still needs a further study. XRD patterns presents that as hydrothermal treatment is longer, a better crystallinity can be achieved, which 24h sample has already

approached closely completed crystallization. On the perspective of reactivity, a better performance of catalytic reaction can be obtained with high crystallinity of ZSM-5.

3.3 EFFECT OF HYDROLYSIS TIME ON POLYDISPERSITY

With the studying of effect of hydrothermal time on crystallinity and crystal size in last chapter, 24h hydrothermal treatment is chosen to be a standard procedure for further investigation. In this chapter, due to the inhomogeneity of crystal size, we aim to modify the synthesis method to produce a well-defined catalyst for further catalyst evaluations.

In the original synthesis adapted from Y. Lai's works[31], the hydrolysis of TEOS could be incomplete due to the relatively short hydrolysis time. Different from hydrothermal reaction which is the step for crystallization, the main function of hydrolysis is to hydrolyze the silica precursor, TEOS. It is reported that the increasing of hydrolysis time will lead to a higher ZSM-5 yield and a slightly decreased crystal size.[35] To ensure complete hydrolysis of TEOS in our case, the hydrolysis time was increased from 2h to 18h.

In addition, according to the SEM images of H-(Fe)ZSM-5 before hydrothermal reaction in Fig. 9(a), it is suspected that the nucleation of amorphous silica in this study has multi-nucleation events which gives rise to inhomogeneous crystal size.[36] This multi-nucleation events typically have a longer time in nucleation stage, which means that some earlier formed particle would grow larger than other later formed particle. By applying the LaMer model[37] which is schematically depicted in Fig. 13, it was anticipated that as the time for nucleation is long enough, Ostwald ripening should provide a self-sharpening growth process which will lead to the uniformity of the final product.[36,38] Ostwald ripening is a thermodynamically-driven process that

smaller particles in solution will dissolve and redeposit onto the surface of larger particles in solution since larger particles are more energetically favored than smaller particles. Consequently, apart from reaching a higher ZSM-5 yield, the enhancement of hydrolysis time should provide ultimately uniform particles as well.

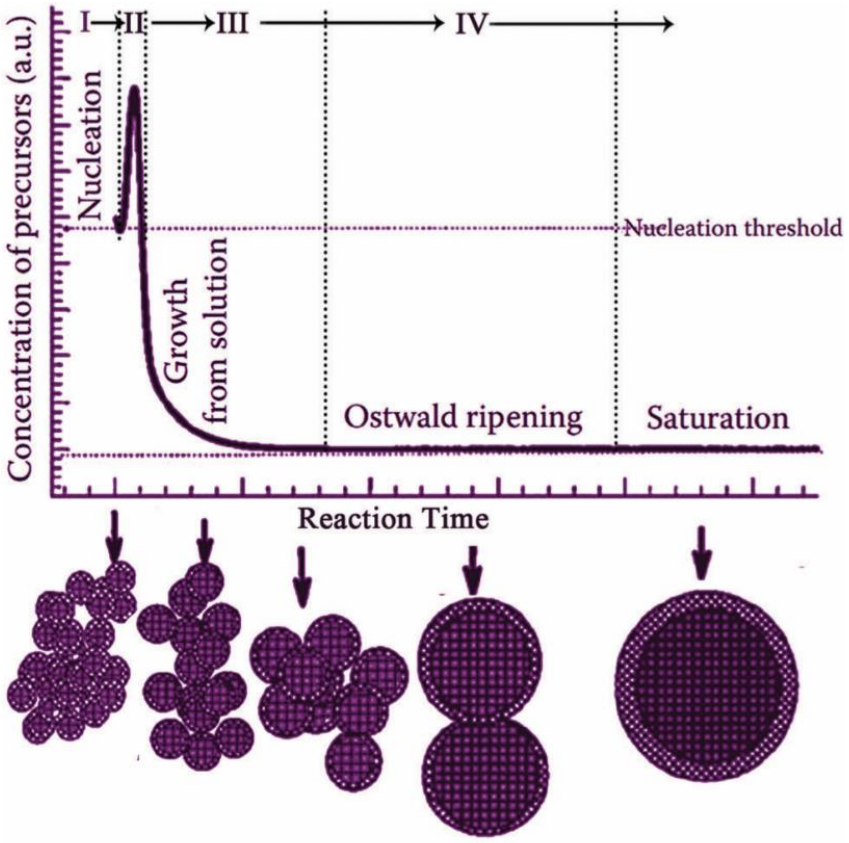

Fig. 13 Graphic description of four stages in nucleation based on LaMer model.[39,40]

3.3.1 Results and discussion

3.3.1.1 Materials characterization

From SEM images shown in Fig. 14, we observed that a longer hydrolysis time will result in more uniform H-(Fe)ZSM-5 particles, which corresponds to our hypothesis above. In addition, particle size distribution chart in Fig. 15 confirms that the size distribution is found to be narrower as the hydrolysis time increase from 2h to 18h. The underlying principle can relate to self-sharpening growth causing from Ostwald ripening in LaMer model mentioned above. An adequate time for hydrolysis of TEOS and nucleation can lead to a saturation stage of particle growth which generate a narrower particle size distribution with a relative large particle size.

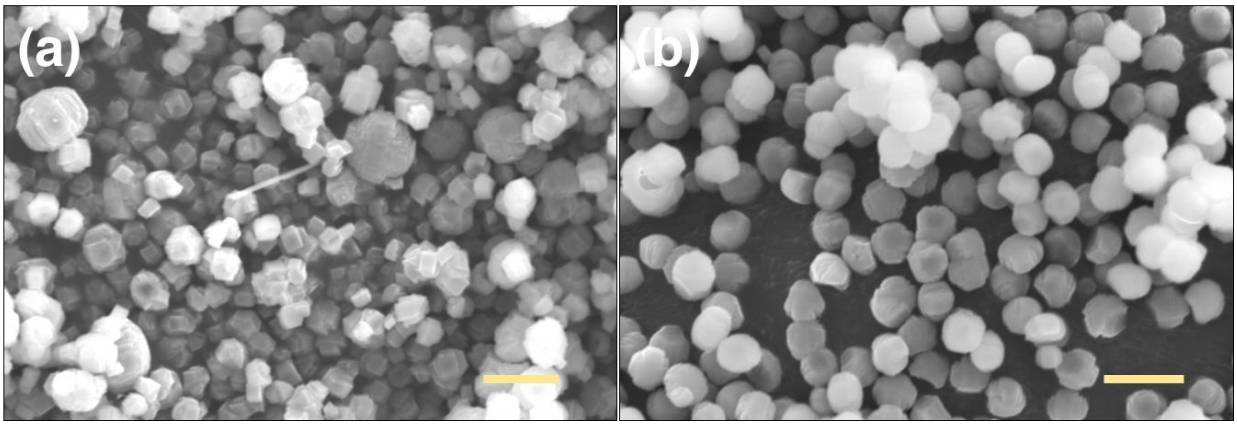

Fig. 14 Scanning electron microscope images of as-synthesized H-(Fe)ZSM-5 with different hydrolysis time: (a) 2h and (b) 18h. Scale bars are 5μm.

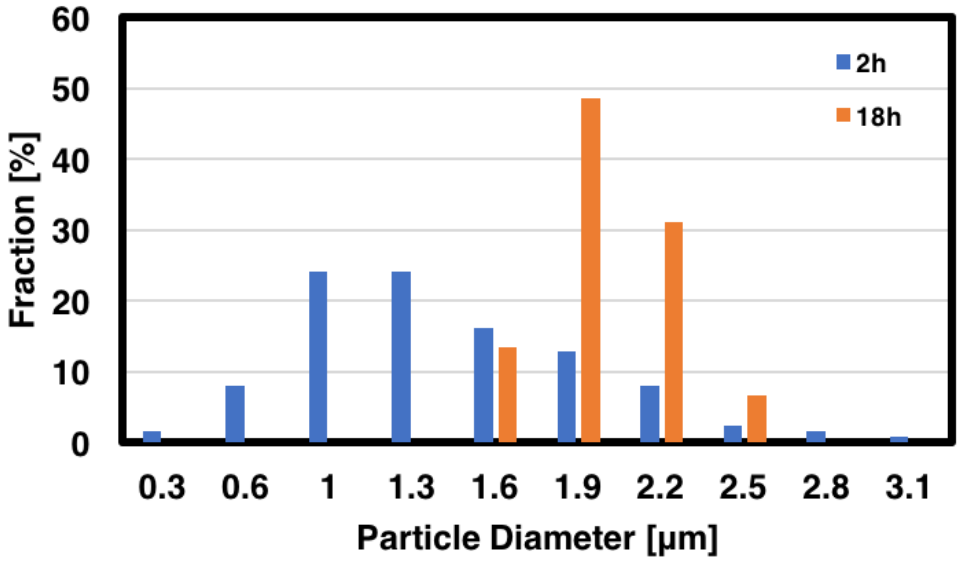

Fig. 15 Particle size distribution diagram: Blue bars represents 2h hydrolysis treatment and orange bar represents 18h hydrolysis treatment.

3.3.2 Conclusion

By increasing hydrolysis time up to 18h, the final product has a narrower particle size distribution and a greater average crystal size. More importantly, more well-defined H-(Fe)ZSM-5 particles were obtained compared to previous results in our lab.[31] However, this increase in hydrolysis time leads to a larger particle size. To study crystal size effect on catalytic activity in DHA reaction, another series of study for effect of template/SiO_2 on crystal size was conducted, which is shown in the next chapter.

3.4 CONTROL OF PARTICLE SIZE VIA VARYING TEMPLATE/SILICA RATIO

For zeolite with microporous structure, nanocrystalline zeolite can have a shorter diffusion pathway for molecules transportation inside zeolite structure, compared to micro-sized zeolites. In DHA, with a shorter molecule diffusion pathway, it will diminish the probability of benzene undergoing secondary reaction and further generate coke inside micro-channels. However, a higher external surface area, one of the distinct properties of nanomaterials, may result in an improved catalytic performance but a faster catalyst deactivation, as discussed in chapter 1.4.1.2.

Tetrapropylammonium hydroxide (TPAOH) serves as a structure directing agent/template to help building up ZSM-5 structure in synthesis solution. TPAOH will be trapped in each channel-intersection of MFI framework. Apart from its templating function, it is reported that the increasing of template concentration will induce a faster nucleation rate of zeolites, and more nuclei formed ultimately lead to the smaller particles.[41–43] Therefore, with changing template/silica ratio, the control of particle size can be achieved. The illustrative diagram of role of TPAOH in nucleation/crystallization is shown in Fig. 16.

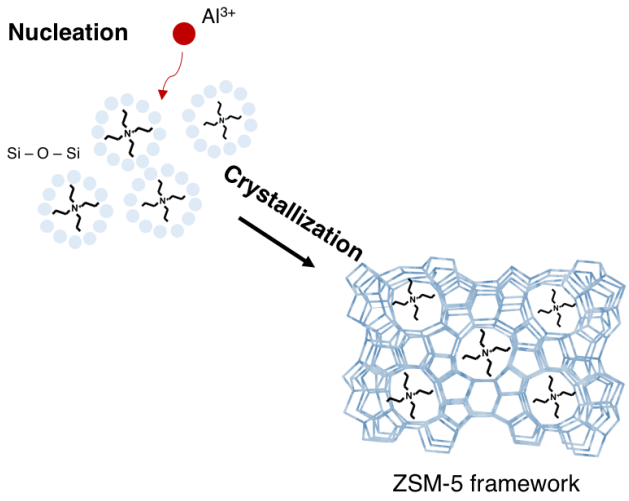

Fig. 16 Schematic role of TPAOH in nucleation step and crystallization step.

However, Persson et al. pointed out that in the case of TPAOH as template, more addition of TPAOH will enhance the alkalinity of the synthesis solution which has a more pronounced influence on particle size.[44] Furthermore, from their statement, utilizing more TPA^+ (from TPABr) does not have any influence on nucleation rate and crystal size. However, this contradiction can probably be attributed to the difference in alkalinity of synthesis solution, which implies that once alkalinity is above a certain threshold, the influence of alkalinity on nucleation rate can be more significant than one from template concentration. Therefore, it would still be worthwhile to study template/silica on crystal size in our synthesis system. Nonetheless, in the case of TPAOH as template, the adding of different amount of template can result in different alkalinity in synthesis solution which will also influence particle growth rate.[44–46] Again, the influence of alkalinity on crystal size seems to be controversial. Persson et al. reported that increasing of alkalinity in synthesis solution will enhance the nucleation rate and form a smaller crystal size, while Fouad et al. and Petushkov et al. found that increasing of alkalinity will produce a larger crystal size. This difference may be related to the presence of Al or not. In the work from Persson et al., the product is synthesized with the absence of Al, while in the case of Fouad et al. and Petushkov et al, aluminum is included in the synthesis. A higher alkalinity in synthesis solution lead to an increase in crystal size, and this can be related to the decrease in the incorporation of Al at high pH and the role of Al species in the nucleation process. [35,43,45] Therefore, to separate the contribution of TPA^+ and alkalinity, in this study, alkalinity is controlled within a pH range from pH 11 to 12. $TPAOH/SiO_2$ ratios were prepared from 0.1 to 0.35 to investigate effect of template/silica ratio on particle size. To balance the alkalinity, the amount of sodium hydroxide in the synthesis was reduced for those samples with

TPAOH/SiO_2 higher than 0.1 since more addition of TPAOH will increase the alkalinity in solution.

3.4.1 Results and discussion

3.4.1.1 Materials characterization

The influence of TPAOH concentration in the synthesis solution on final crystal size is shown in Fig. 17. It shows that the crystal size decrease from 2700nm to 300nm when TPAOH/SiO_2 is increased from 0.1 to 0.35. The average particle size calculated are shown in Table 2. With minimizing the contribution of alkalinity, in our case, TPA^+ does play a role in influencing the ultimate crystal size which agree with the work from Crea et al.[41] Moreover, it is found that the morphology of H-(Fe)ZSM-5 is different between template/silica ratio = 0.1 and the other samples, which sample containing sodium has a cross-like shape whereas samples without adding sodium have a elliptic-like cylinder, which would be discussed more explicitly in chapter 3.5.

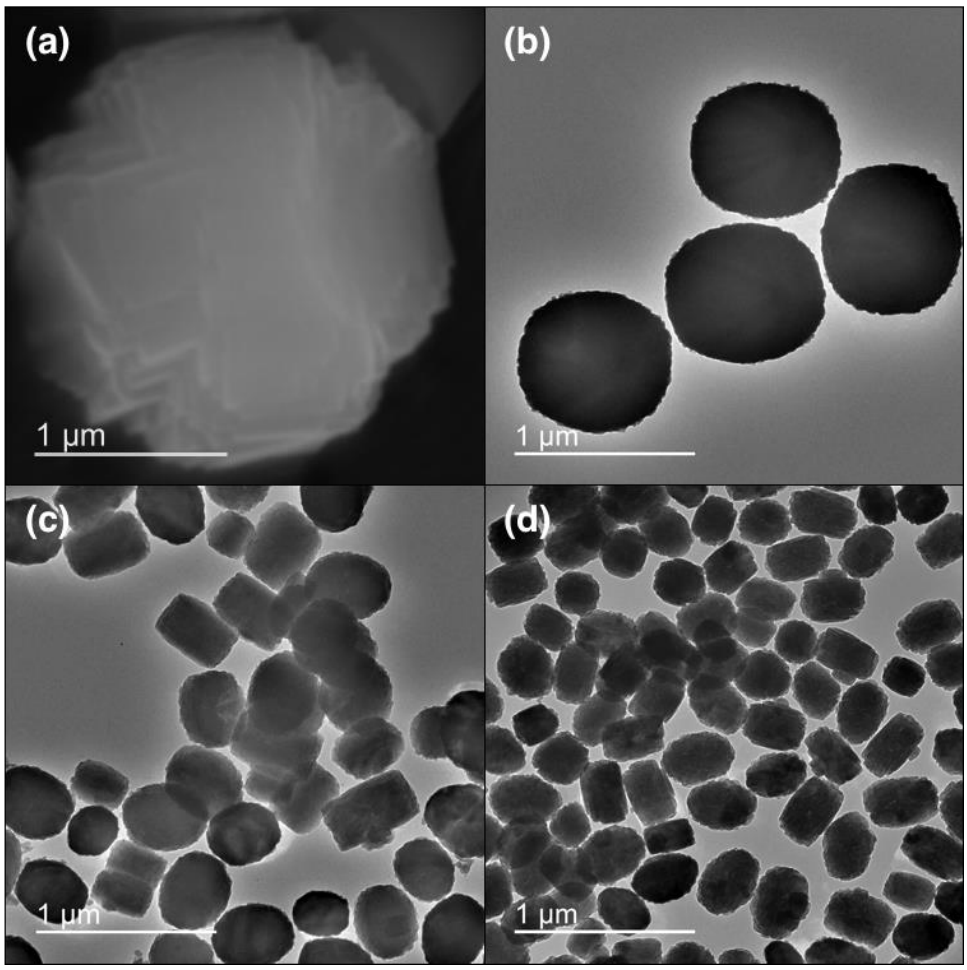

Fig. 17 Scanning electron microscope image and transmission electron microscope images of H-(Fe)ZSM-5 sample with different template/silica ratio: (a) 0.1, (b) 0.2, (c) 0.27 and (d) 0.35

In this study, the investigation on crystallinity is also necessary since it's known that both the introduction of sodium and the changes in alkalinity can influence the crystallinity[35], which may further affect the catalytic performance. From XRD pattern in Fig. 18, based on the intensity, the absence of sodium in synthesis solution may increase the crystallinity slightly, and the increase in alkalinity seems to decrease the crystallinity, which is probably caused by the change of particle size. However, comparing to one with 120 hydrothermal treatment in chapter 3.2, which is expected to be fully crystallized, these four samples are considered to be

completely crystallized as well. Therefore, crystallinity is expected to be uninfluential in this chapter.

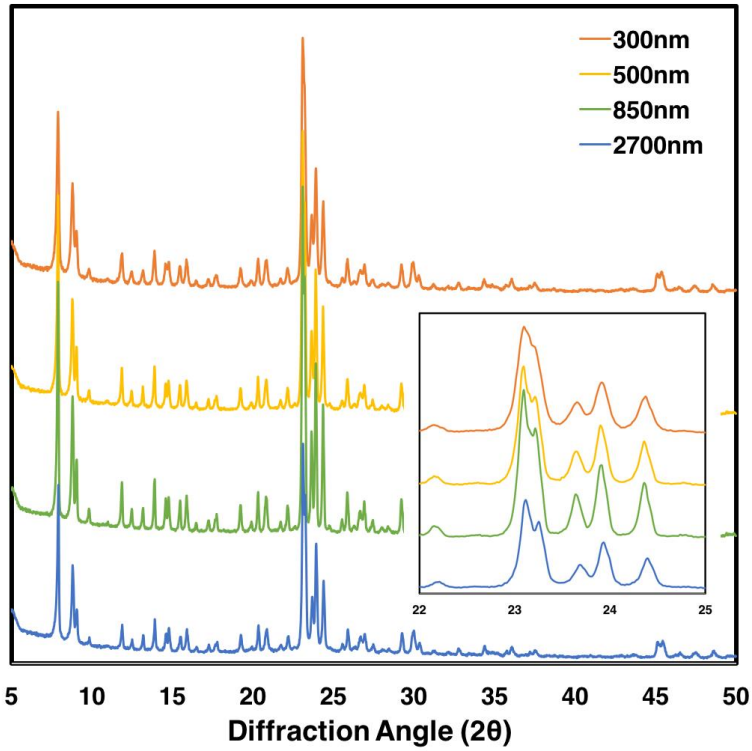

Fig. 18 X-ray diffraction pattern of as-synthesized H-(Fe)ZSM-5 with different template ratio. TPAOH/SiO2 = 0.1, 0.2, 0.27 and 0.35 refer to 2700nm, 850nm, 500nm and 350nm, individually.

In addition to crystal morphology analysis and crystallinity analysis, analysis of surface area can be supportive information especially in this series of controlling particle size. Some interesting findings were observed in the surface area/porosity analysis. Fig. 19 shows porosity analysis of H-(Fe)ZSM-5 with various template/silica ratio. From N_2 adsorption/desorption isotherm in Fig. 19(a), it is obvious that 2700nm sample has a very different adsorption/desorption behavior from the other samples. 2700nm sample has a hysteresis which

has an enclosed point around P/P_0 = 0.45. This phenomenon is so called "Tensile Strength Effect" due to the formation of ink bottle shape of pores which has a smaller pore throats.[47] Accordingly, the peak around 4 nm observed from BJH desorption branch is an artifact and does not represent a real pore distribution, which is instead measured from the desorption data, shown in Fig. 19(c).[48] In this condition that adsorption branch is not matched with desorption branch, which cause the hysteresis, it is generally accepted that adsorption branch can be the only reliable data for pore analysis since adsorption branch is not affected by tensile strength effect.[49] From Fig. 19(b), BJH adsorption branch presents that 2700nm sample has a very board peak located from 4nm to 25nm. In addition, the mesopore volume from 4-100nm in Table 2 were calculated from BJH adsorption branch, which also suggests that 2700nm sample has the highest mesopore volume. Different from mesoporosity of the other samples, these mesopores in 2700nm sample may exist in a form of ink bottle shape which usually leads to the more obvious influence of Tensil Stength Effect in N_2 adsorption/desorption. Apart from 2700nm sample, as particle size decrease from 850nm to 300nm, the mesoporose volume increase which may be contributed by the slightly increased alkalinity, which is also shown in Table 2.[46]

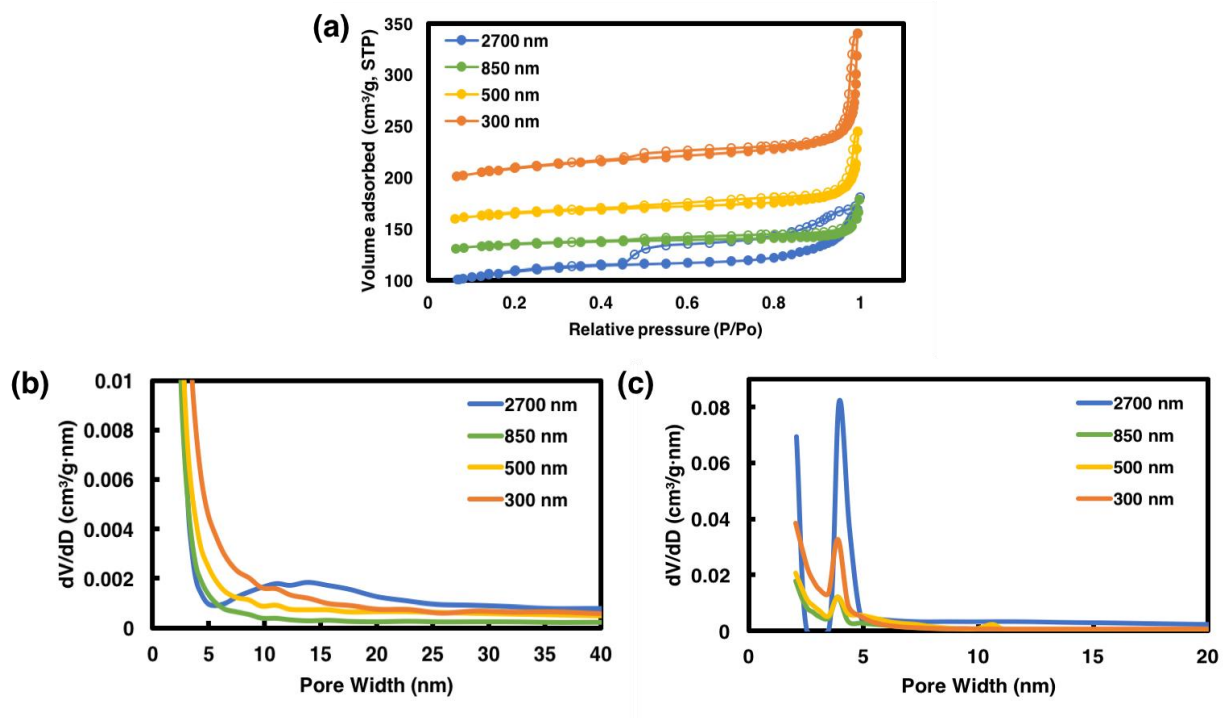

Fig. 19 (a) N2 adsorption and desorption isotherms at 77K: enclosed symbol refers to adsorption and open symbol refers to desorption, (b) BJH mesopore size distribution taken from adsorption branch and (c) BJH mesopore distribution taken from desorption branch.

Table 2 presents the synthesis condition, surface area and mesoporosity of each sample. Intriguingly, comparing 2700nm sample and 500nm sample which are synthesized under a close pH, it reveals that the addition of sodium has a certain influence on generating mesoporosity inside ZSM-5, which is barely described in literatures. The only hint coming from Itani et al. is that during the induction period, sodium penetrates inside aluminosilicate species by breaking their structure.[50] Except this statement, it seems that no literature discusses about the effect of sodium on mesoporosity. In addition, it is also found that the increasing of alkalinity from template/silica ratio = 0.2 to 0.35 still give rise to the growing mesoporosities from 0.024 cm^3/g to 0.072cm^3/g.

Table 2 Materials properties of H-(Fe)ZSM-5 with different template/silica ratio.

TPAOH/SiO_2	pH	Solution before Crystallization	Average size[nm]	S_{BET} [m^2/g]	$V_{meso,\ 4\text{-}100nm}$ [cm^3/g]
0.1	11.3	Opaque	2700	430.9	0.078
0.2	10.9	Clear	850	358.6	0.024
0.27	11.2		500	360.5	0.049
0.35	12.2		300	425.6	0.070

3.4.1.2 Catalytic performance

In terms of reactivity, Fig. 20(a) shows the methane conversion of H-(Fe)ZSM-5 with various template/silica ratio. Unexpectedly, the sample with TPAHO/SiO_2 = 0.1 and the biggest particle size has similar performance as the one with the smallest particle size, and the gap between 2700nm sample and 850nm sample cannot be explained via particle size effect. Additionally, a huge improvement is observed from 900nm sample to 500nm sample but there is no significant difference between 500nm particle and 300nm particle. The similar scenarios are shown in Fig. 20(b), (c) and (d), which except TPAOH/SiO_2 = 0.1, benzene selectivity/yield/production results that show a systematic increase in selectivity/yield/concentration is found as particle size decrease. For this unexpected trend, the influence of crystallinity is considered to be negligible here since all these samples are fully crystallized. One possible explanation is that the formed mesoporosity in 2700nm sample enhance the catalytic performance. Returning to TPAOH/SiO_2 = 0.1, the only synthetic difference between this sample and the other samples is the addition of sodium hydroxide in order to control alkalinity, shown in Table 2. Moreover, coupled with mesopore volume shown in table 2, the trend in catalytic results seems to agree very well with the trend of mesoporosity. Interestingly, comparing the catalytic performance

between 2700nm sample and 300nm sample, it is concluded that effect of particle size on catalytic performance is not as significant as mesoporosity is.

Overall, the trend in mesoporosity can reasonably justify our observations in catalytic performances. Additionally, it is suggested that the impact of mesoporosity on reactivity is more pronounced than one from particle size.

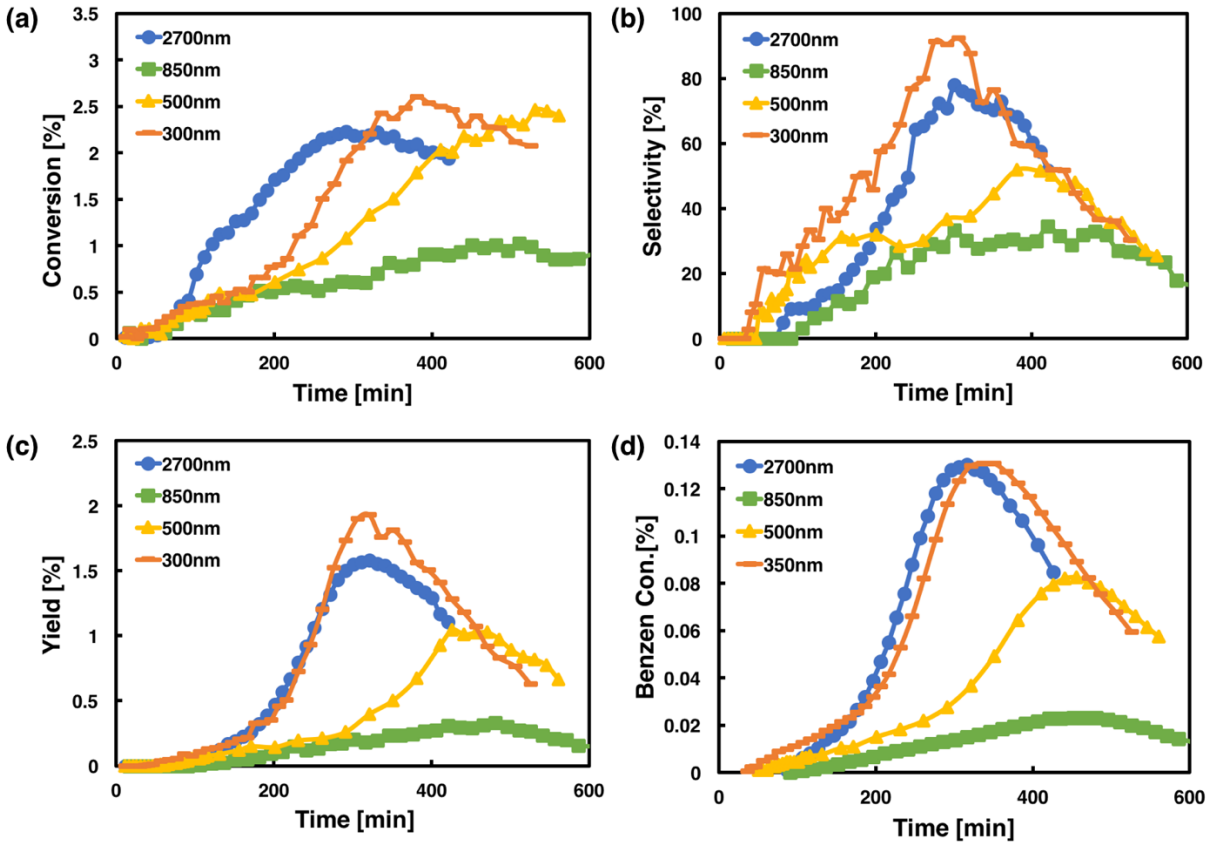

Fig. 20 Reactivity data of samples with different template/silica ratio: (a)CH_4 conversion, (b) C_6H_6 selectivity, (c) C_6H_6 yield and (d) C_6H_6 concentration. TPAOH/SiO_2 = 0.1, 0.2, 0.27 and 0.35 refer to 2700nm, 850nm, 500nm and 350nm, individually.

3.4.2 Conclusion

To investigate the particle effect on catalytic performance, we successfully controlled the particle size by changing template/silica ratio. Four samples with different TPAOH/SiO_2 ratios were synthesized with controlled synthesis pH in order to separate the effect of pH from TPA^+. SEM and TEM images confirmed the crystal shrinking trend and morphology changes of H-(Fe)ZSM-5 with various template/silica ratios. However, the change in particle size cannot explain the trend of catalytic performance appropriately. On the other hand, porosity analysis provides an insight that the addition of sodium, which is originally to balance synthesis pH, or slightly elevated synthesis pH will give rise to the formation of mesoporosity. Furthermore, the trend of mesoporosity provides an explanation for what we observed in catalytic results. Therefore, the changes in reactivity results are considered to be mainly affected by the formed mesoporosity, which implies that the particle size effect on catalytic activity is insignificant comparing to the impact of mesoporosity on reactivity.

3.5 EFFECT OF SODIUM ON MESOPOROSITY

In zeolite synthesis system utilizing TPA^+, the function of sodium is quite complicated. Persson et al. demonstrated that the increase in sodium amount can induce a faster crystal growth rate due to its role as charge compensators which make incorporation of aluminum easier.[51] Additionally, Yan et al. reported that the presence of Na^+ in ZSM-5 synthesis system using TPA^+ is to decrease

both nucleation rate and crystallization rate and have multifaceted effect on crystal morphology.[52–54] The possible explanation for Na^+ to cause the decrease of both nucleation rate and crystallization rate is that Na^+, being a positive ion, will compete with larger molecule TPA^+ to occupy the surface of silica precursor, which makes TPA^+-silica surface reduced.[54] The results from Persson et al. seems to be contradictory to the conclusions from later literature. This argument can possibly be considered as the difference in amounts of Na^+ and TPA^+ used. When Na^+ is above a certain threshold, the competition between TPA^+ and Na^+ becomes significant, whereas low amount of Na^+ should make the incorporation of Al^- easier without severe struggling. However, there is no literature reported that sodium ion would affect porosity. In last chapter, we found that Na^+ have certain impact on meso-porosity which contributes to the hysteresis in Langmuir isotherm in Fig. 19(a).

In this chapter, we aimed to examine how mesoporosity is influenced by the addition sodium ion in ZSM-5 synthesis. First, to distinguish the effect of sodium from alkalinity, three samples with different alkalinity and w/ or w/o Na^+ were synthesized. Secondly, it was expected that if Na^+ can be added right before hydrothermal reaction (after hydrolysis), the final particle size should be much smaller since it won't induce the fast nucleation in synthesis solution. In this case, zeolite with small size and mesopores should be obtained. With this idea, H-(Fe)ZSM-5 with a much better catalytic performance can be expected. Hence, samples with adding Na^+ before/after hydrolysis time were made. Moreover, by comparing addition of Na^+ before hydrolysis and after hydrolysis, it should give us an insight which step (hydrolysis step or hydrothermal step) will Na^+ induce mesoporosity, which will help us to come up with the hypothesis for how Na^+ induce mesopore formation. For example, if mesoporsity only formed in the condition of adding Na^+ before hydrolysis, it means that mesopore formation only occurs in

nucleation step (hydrolysis step). The synthesis condition is shown in table 3. In this trial, sodium nitrate is used as the source of sodium which can separate alkalinity effect from sodium effect and compensate the enhanced alkalinity caused by TPAOH.

3.5.1 Results and discussion

3.5.1.1 Materials characterization

From Langmuir isotherm diagram in Fig. 21(a), it is obvious that only the addition of sodium before hydrolysis would have the ability to create a pronounced hysteresis. In addition, increased alkalinity also creates a small degree of hysteresis, which is also observed in last chapter. However, intriguingly, comparing the introduction of sodium before/after hydrolysis, it is found that only the addition of Na^+ before hydrolysis seems to generate mesopores. From BJH adsorption branch in Fig. 21(b), H-(Fe)ZSM-5 with the addition of Na^+ before hydrolysis does have a relatively broad peak from around 5nm to 40mn, which further confirmed that sodium is the key element to form this mesoporosity. The detailed cause for the presence of Na^+ to generate mesoporosity still requires a systematic study for its role in nucleation. Since the addition of Na^+ after hydrolysis does not affect mesoporosity which means that the step of forming mesoporosity is not crystallization step. As mentioned in chapter 3.4.1.1, the only hint that can find in literature is that sodium will penetrates inside aluminosilicate species via breaking their structure.[50]

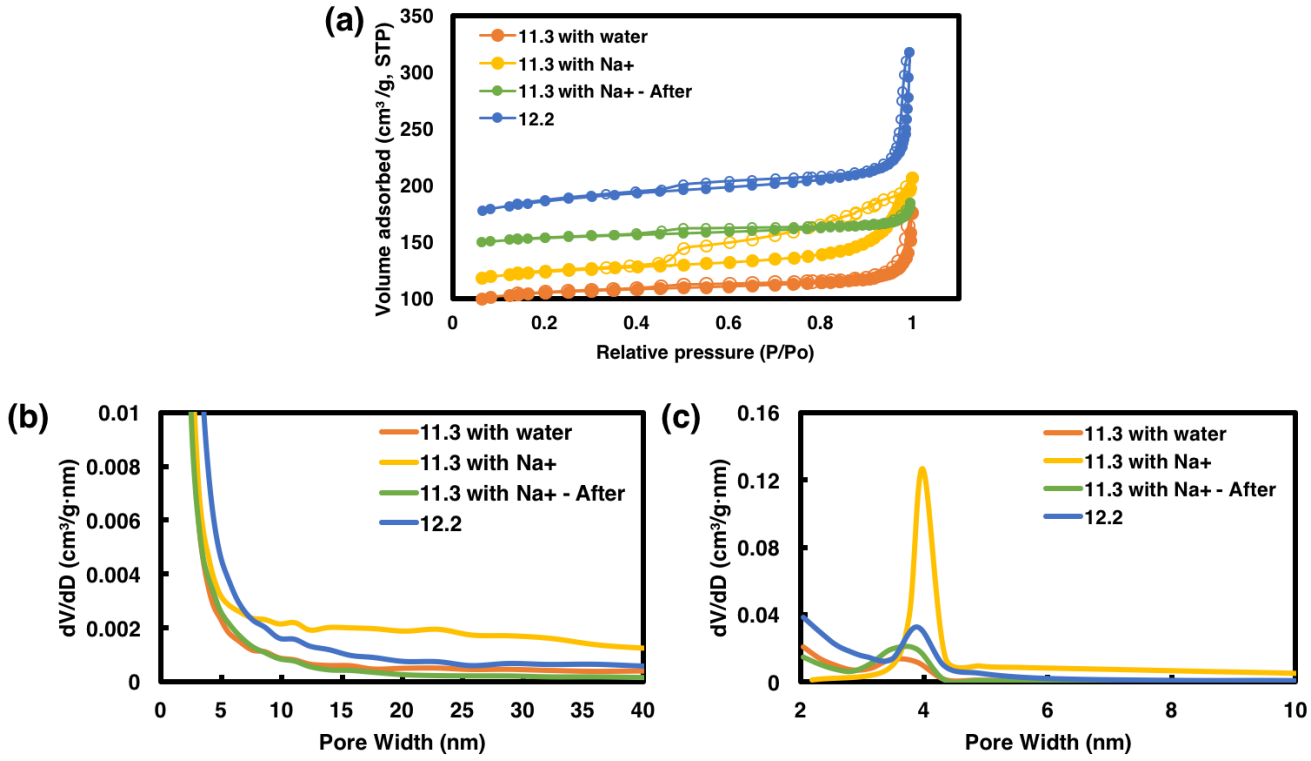

Fig. 21 Porosity analysis of H-(Fe)ZSM-5 with different synthesis condition: (a) N_2 adsorption and desorption isotherms at 77K: enclosed symbol refers to adsorption and open symbol refers to desorption, (b) BJH mesopore size distribution taken from adsorption branch and (c) BJH mesopore distribution taken from desorption branch.

The detailed synthesis condition and porosity properties are shown in table 3. It is found that from the calculated mesopore volume, samples with enhanced alkalinity and the addition of Na^+ have a similar mesopore volume while the latter condition can have a more pronounced hysteresis in N_2 adsorption/desorption diagram, which may imply the difference in pore morphology.[48] Interestingly, Fig. 22 shows that the consequence of adding Na^+ before hydrolysis was forming an opaque solution which visible particles had formed whereas the adding of Na^+ after hydrolysis resulted in a clear solution which implies either the absence of particles or

containing nuclei that are smaller than the wavelength of visible light. This difference may indicate that an introduction of sodium into an incomplete hydrolysis synthesis solution can lead a destabilization of silica-aluminate and further force the nucleation while a same scenario won't happen in a complete hydrolysis synthesis solution. This phenomenon which Na^+ will destabilize (alumino)silicate solutions is also reported by Persson et al.[51]

Table 3 Material properties and synthesis condition of H-(Fe)ZSM-5 with template/silica ratio but different synthesis condition.

$TPAOH/SiO_2$	pH	Sodium	H_2O	Solution before Crystallization	S_{BET} [m^2/g]	$V_{meso,\ 4\text{-}100nm}$ [cm^3/g]
0.35	11.3	/	Adding before hydrolysis	Clear	394.6	0.040
0.35	11.3	Adding before hydrolysis	/	Opaque	417.2	0.071
0.35	11.2	Adding after hydrolysis	/	Clear	347.5	0.027
0.35	12.2	/	/	Clear	425.6	0.070

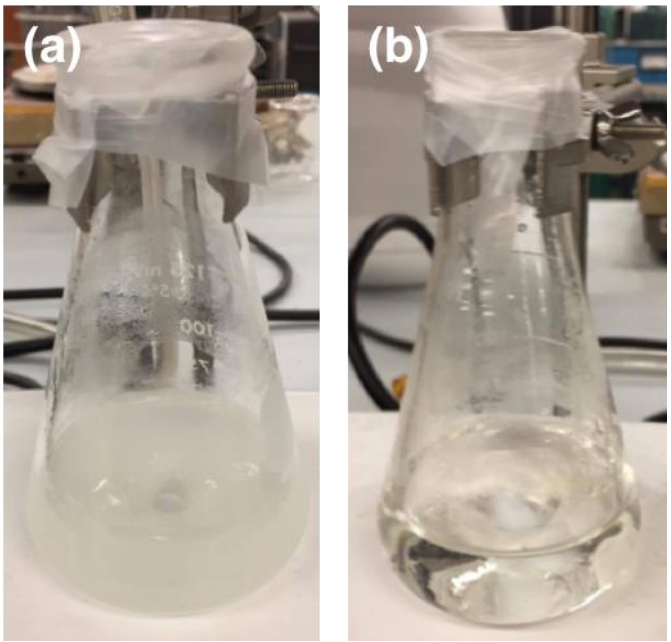

Fig. 22 Demonstration of synthesis solutions: (a) Opaque solution (b) Clear solution.

Because of earlier nucleation in the synthesis condition of adding Na^+ before hydrolysis, it will lead to a bigger particle size comparing to adding Na^+ after hydrolysis, as shown in Fig. 23(b) and (c). In the other words, the nanocrystalline ZSM-5 cannot be obtained with presence of Na^+, which is also confirmed by Van Grieken et al.[35] More interestingly, comparing Fig. 23(a) and (d) with (b) and (c), morphology of ZSM-5 will also be changed with the addition of Na^+, no matter what the adding sequence is. Taking $TPAOH/SiO_2 = 0.1$ in last chapter as an example, the morphology of crystal is a cross-like particle whereas those samples without addition of sodium are much closer to elliptic cylinder. Unfortunately, this morphology change induced by Na^+ is still need a further study. Typically, the commercial ZSM-5 will have the morphology close to elliptic cylinder. This probably indicates that the presence of Na^+ will interfere the crystal facet growth rate and ultimately lead to the morphology consisted of two-intergrowing crystals.

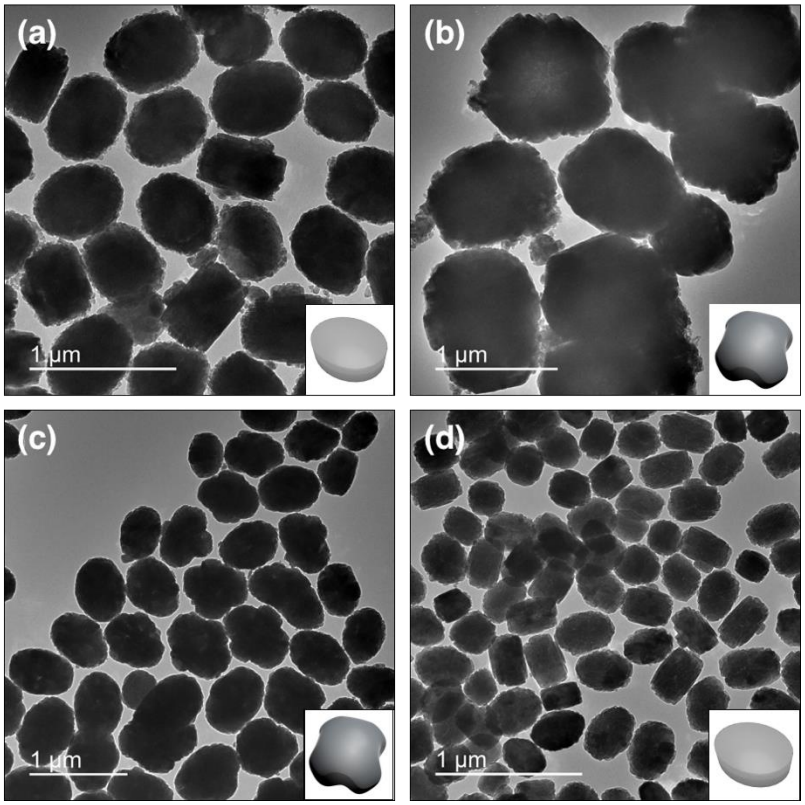

Fig. 23 Transmission electron microscope images of H-(Fe)ZSM-5 with different synthesis condition: (a) pH=11.3 with addition of water, (b) pH=11.3 with addition of $NaNO_3$ before hydrolysis, (c) pH = 11.2 with addition of $NaNO_3$ after hydrolysis and (d) pH=12.2 without any modification. Illustrative morphologies of each sample were shown in bottom right.

3.5.2 Conclusion

So far, there are only few literature reporting that sodium ion in ZSM-5 synthesis has influence on nucleation rate, crystal growth rate and crystal morphology.[51–53,55] However, no literature reported explicitly that sodium has effect on creating mesopores which is observed in chapter 3.4. The reason can probably be attribute to that Na^+ will penetrate the structure of aluminosilicate.[50] Four samples with different synthesis condition were made to investigate the effect of sodium ion on porosity. From porosity analysis, it is found that the only condition to

form hysteresis in N_2 adsorption/desorption diagram is the addition of Na^+ before hydrolysis, which means that step of forming mesoporosity occurs at this hydrolysis step (nucleation step). Additionally, the increment of alkalinity would also result in a comparable amount of mesopore while it does not cause a distinct hysteresis as the addition of Na^+ before hydrolysis does. From SEM images, we also observed that addition of Na^+ in any sequence will have a different crystal morphology comparing to ones without addition of Na^+, which implies that sodium will induce a multifacet growth of crystal during the crystallization step. Although the amount of pore volume created by Na^+ is relatively small compared to those one created by post-synthesis, it can still make a non-negligible difference in catalyst performance, which is discussed in chapter 3.4. With this idea, different amounts of mesopores probably can be generated from adding various amounts of Na^+ into synthesis solution, which can potentially give rise to a better catalyst for DHA. In addition, with the ability to control mesoporosity in ZSM-5, we aimed to revisit how does particle size exclusively affect catalytic performance.

3.6 CONTROL OF PARTICLE SIZE WITH FIXED MESOPOROSITY VIA CHANGING TEMPLATE/SILICA RATIO

As discussed above, from our results, it shows that Na^+ plays an important role in forming mesopores within zeolite. In order to investigate the exclusive effect of particle size on reactivity, both amount of Na^+ and alkalinity need to be maintained. With identical amount of Na^+ and same pH value, the mesoporosity should be the similar and not be a variable in this case. To keep pH value in a close value and maintain the amount of sodium in synthesis solution, different amount

sodium nitrate were added into those synthesis solutions with $TPAOH/SiO_2$ above than 0.1, which the detailed synthesis condition is shown in table 4.

3.6.1 Results and Discussion

3.6.1.1 Materials characterization

Synthesizing with fixed amount of Na^+ and different template/silica ratio, various size of ZSM-5 should have the similar mesoporosity. However, the introduction of Na^+ will limits the decreasing of particle size. The addition of sodium will result in an opaque synthesis solution in which amorphous silica has already formed, which is shown in Fig. 10. Fig. 24 shows the SEM images of H-(Fe)ZSM-5 with introduction of Na^+ and $TPAOH/SiO_2$ from 0.07 to 0.2. Generally, it shows that as template/silica ratio increase, the average crystal size would decrease, similar to the results in chapter 3.4. However, when $TPAOH/SiO_2$ is above 0.2, the influence of increasing TPA^+ is mitigated if $TPAOH/SiO_2$ is below 0.07, the products tend to be more polydisperse, which is shown in appendix A. This result probably can be relate to the fact that the synthesis solution will be transformed into a gel-like mixture if $TPAOH/SiO_2$ is below 0.07. The relative slow nucleation rate due to the less TPA^+ concentration is not likely to be the explanation because a small change in template/silica ratio should not be that sensitive, which the sample with $TPAOH/SiO_2 = 0.07$ is still monodisperse. Hence, the product of H-(Fe)ZSM-5 with $TPAOH/SiO_2$ below 0.07 is not considered within this chapter in order to keep the synthesis condition (in form of solution) identical.

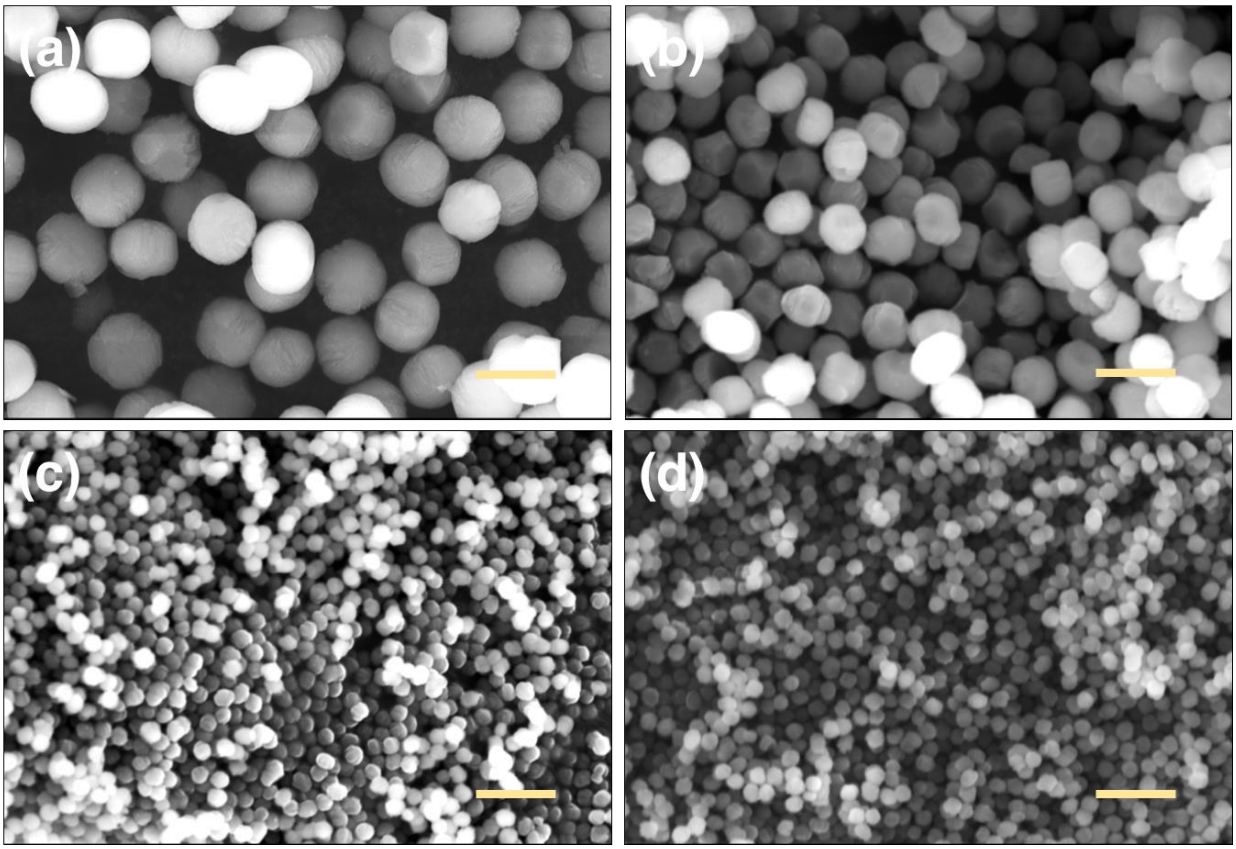

Fig. 24 Scanning electron microscope images of H-(Fe)ZSM-5 with different template/silica ratio but the same amount of Na^+ addition: (a) $TPAOH/SiO_2 = 0.07$, (b) $TPAOH/SiO_2 = 0.1$, (c) $TPAOH/SiO_2 = 0.15$ and (d) $TPAOH/SiO_2 = 0.2$. All scale bars are 5μm.

In Fig. 25(a), the N_2 adsorption-desorption isotherm for these samples are typically type IV isotherm with type H2 hysteresis. With introduction of comparable amount of sodium, these samples all have similar hysteresis phenomenon which is caused by tensile strength effect. Moreover, BJH adsorption branch in Fig. 25(b) shows that there are broad mesopores formed within these samples. Then, from BJH desorption branch in Fig. 25(c), as expected, peak from tensile strenth effect occurs in all samples, which does not represent true pore size distritubtion. And the calculated mesopore volume is shown in table 4, which shows that with a fixed amount

of Na^+ introducing, a comparable amount of mesopore volume can be reached. These results further implies that with controllable amount of Na^+, the mesopore volume can possibly be tunable.

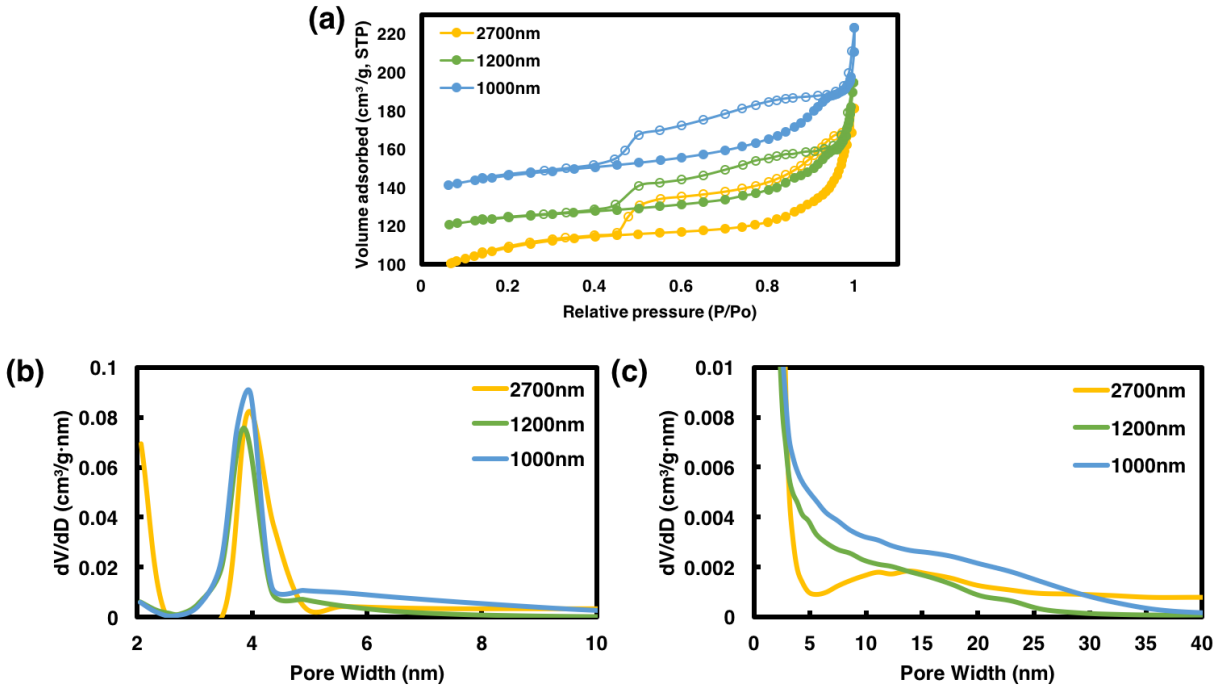

Fig. 25 Porosity analysis of of H-(Fe)ZSM-5 with different template/silica ratio but the same amount of Na^+ addition: (a) N_2 adsorption and desorption isotherms at 77K: enclosed symbol refers to adsorption and open symbol refers to desorption, (b) BJH mesopore size distribution taken from adsorption branch and (c) BJH mesopore distribution taken from desorption branch. $TPAOH/SiO_2$ = 0.1, 0.15 and 0.2 refer to 2700nm, 1200nm and 1000nm, individually.

Table 4 Materials properties and synthesis condition of H-(Fe)ZSM-5 with different template/silica ratio but the same amount of Na^+ addition.

TPAOH/SiO_2	pH	Amount of Na^+ [mmol] NaOH / $NaNO_3$	Solution before Crystallization	Average Size [nm]	S_{BET} [m^2/g]	$V_{meso,\ 4\text{-}100nm}$ [cm^3/g]
0.07	11.0	6.67 / 0	Opaque	4300	-	-
0.1	11.3	6.67 / 0		2700	430.9	0.078
0.15	11.2	5 / 1.67		1200	453.1	0.071
0.2	11.1	3.75 / 2.92		1000	465.2	0.077

3.6.1.2 Catalytic Performance

Returning to reactivity studies, CH_4 conversion in Fig. 26(a) clearly shows that as particle size decrease, both catalytic activity and selectivity increase gradually, and the time reached maximum value gets longer which means the decreasing of particle size extend the induction period of catalyst. This induction period-extending implies that the rate of activating methane on Fe is slower when particle size decrease. It also means that a certain transformation occurs on Fe site, which is related to the change in particle size. The detail of this mystery still need a further investigation. However, the deactivation rates in methane conversion among these samples have no obvious difference, which means coke formation does not change with decreasing of particle size. From Fig. 26(b), (c) and (d), it also shows the similar trend in benzene yield/selectivity/production while 1000nm sample has a slightly lower benzene selectivity comparing to 1200nm, which combines its higher conversion to give a similar benzene production. From these catalytic evaulation, we can conclude that in these particle size range, the decreasing of ZSM-5 particle size will result in a enhancement on catalytic activity and product selectivity of catalyst. Cui et al. also studied effect of particle size on reactivtiy of Mo/ZSM-5 in

DHA.[25] In their case, acidity and crystallinity of ZSM-5 were changed because mechanical breaking down cause the structure breakage of ZSM-5 crystal. Therefore, the reactivity results they presented cannot be attributed to the sole effect of zeolite particle size.

Comparing to the results in chapter 3.4, although the absence of sodium can enable the formation of nanocrystalline H-(Fe)ZSM-5 (d~300nm), a rather bigger size of H-(Fe)ZSM-5 (d~1000nm) with mesoporosity created from the addition of sodium can have a greater benzene yield. Again, this result probably confirmed that the influence of mesoporosity can be more significant in catalytic performance than one from particle size. From chapter 3.4, the change in mesopore amount give rise to a drastic change in CH_4 conversion, which is shown in Fig. 20, while the change in particle size in this chapter does not lead to the comparable impact on reactivtiy as we observed in chapter 3.4.

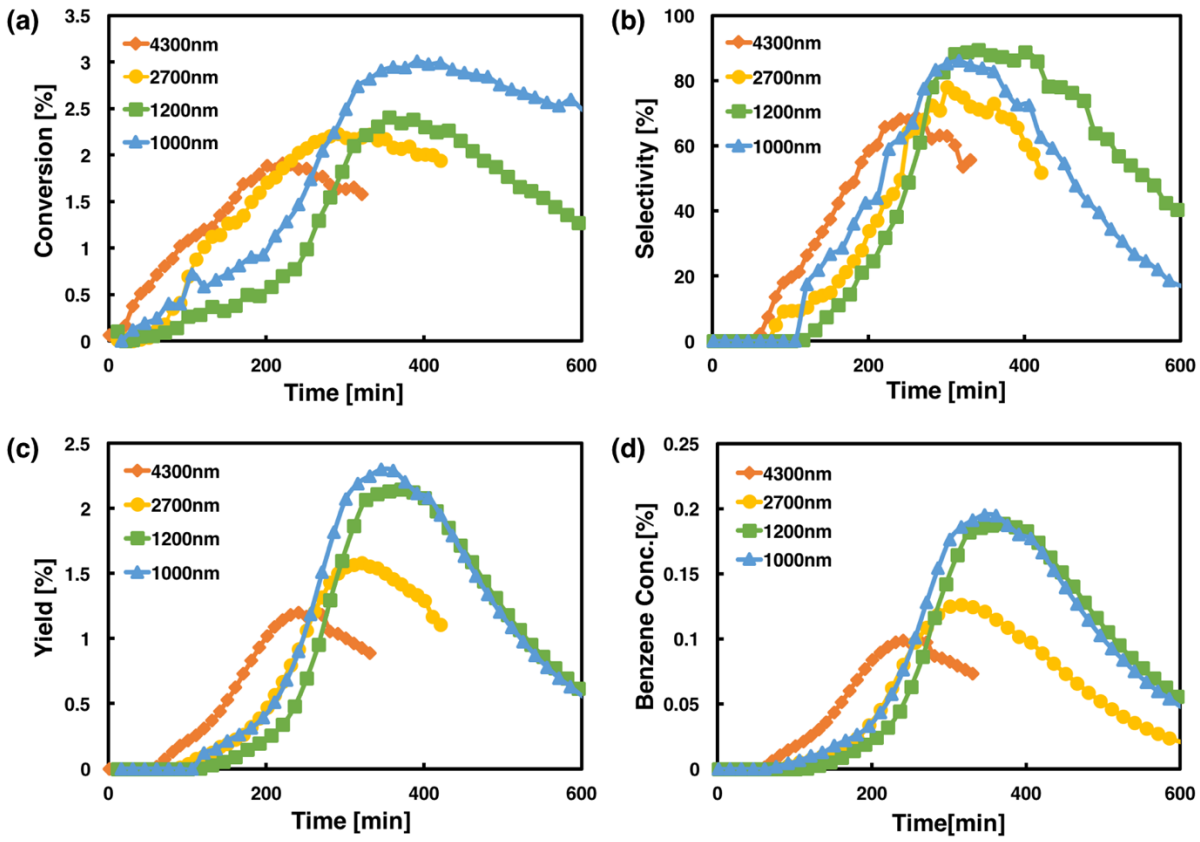

Fig. 26 Reactivity data of samples with different template/silica ratio but the same amount of Na^+ addition: (a)CH_4 conversion, (b) C_6H_6 selectivity, (c) C_6H_6 yield and (d) C_6H_6 concentration. $TPAOH/SiO_2$ = 0.07, 0.1, 0.15 and 0.2 refer to 4300nm, 2700nm, 1200nm and 1000nm, individually.

3.6.2 Conclusion

With the fixed total amount of Na^+ and alkalinity, four samples were synthesized to investigate how catalytic performance is affected by ZSM-5 particle size. SEM images show a similar trend as in chapter 3.4 that as template/silica ratio increase, the crystal size would decrease. Porosity analysis presents that a con trolled amount of Na^+ can lead to a comparable mesoporosity which allow us to study the only effect of crystal size. From reactivity results, it is shown that in the case of fixed mesoporosity, smaller particle can indeed enhance the production of benzene.

Nonetheless, compared to the results in chapter 3.4, we concluded that mesoporosity can have more pronounced impact on catalytic performance than particle size does. More importantly, we also showed that the introduction of Na^+ is the key component for zeolite to form inherent mesopores which can help increase catalytic activity and the production of benzene.

3.7 FUNCTIONALITY OF EXTERNAL BRONSTED ACID SITE

In catalytic reaction, zeolite provides not only shape-selectivity from its framework but also catalytic activity which is resulted from acidity. However, for acid sites, only those acid sites located inside zeolite channels will participate the reactions under a shape-selective environment. On the contrary, acid sites on the external surface of zeolite are easier to expose to reactants and undergo non-selective reactions due to the absence of spatial confinement, which may lead to the faster formation of coke and large hydrocarbons.[56–58] Therefore, the passivation of external Bronsted acid site is considered as a way to reduce the coke formation and enhance the product selectivity, which not only extend the catalyst lifetime but also improve the catalyst performance.

For DHA reaction, Ding et al. reported that silanation of external acid sites of Mo/HZSM-5 can boost the reaction rate and decrease the catalyst deactivation rate since the reaction occurred preferentially in the shape-selective environment.[56] In addition to directly passivating the Bronsted acid site on external surface of zeolites, over-growth type mesoporous silica on the zeolites is an alternative way to inhibit the direct contacting of acid sites and reactive species.[59–61] Qian et al. demonstrate that a thin mesoporous silica shell(~20nm) can be successfully deposited on ZSM-5.[60] More importantly, they also show that the silica deposition on ZSM-5 has a negligible impact on the kinetic diffusion of benzene molecule, which kinetic

diffusion efficiency for silica coated ZSM-5 is ~$7.25\times10^{-19}m^2s^{-1}$ while one for parent ZSM-5 is ~$7.88\times10^{-19}m^2s^{-1}$. In this study, we follow the method from Qian et al. to deposit a thin silica layer(~75nm) on the H-(Fe)ZSM-5 made before, and the catalytic performance of this silica deposited H-(Fe)ZSM-5 is evaluated by DHA reaction. And, a brief schematic of the synthesis method of SiO_2 is shown in Fig. 27.

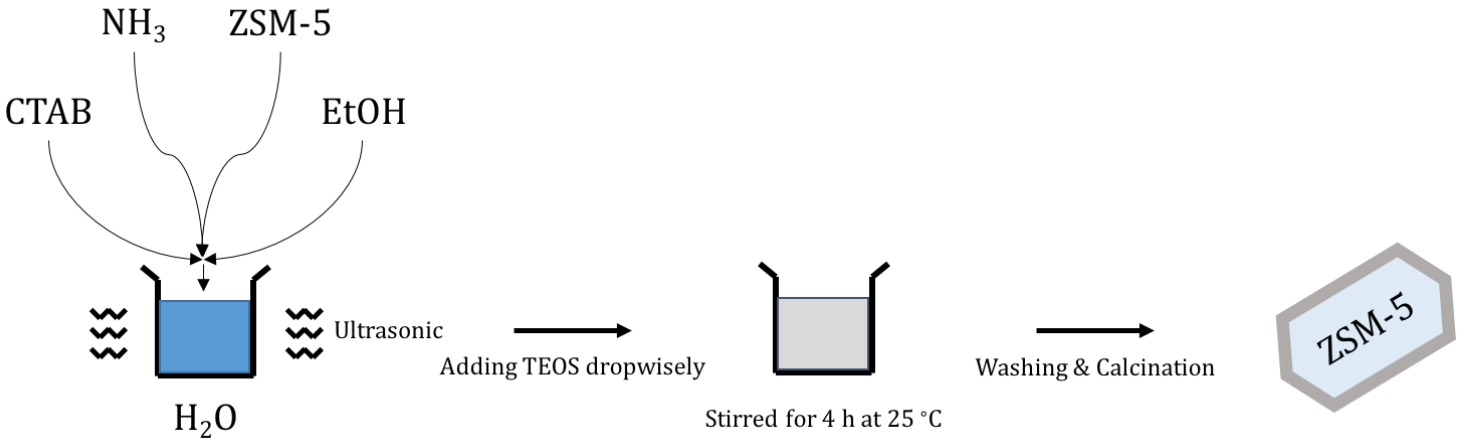

Fig. 27 Illustration of synthesis method for SiO_2 growth on ZSM-5.[60]

3.7.1 Results and discussion

3.7.1.1 Materials characterization

To compare the morphology and thickness of SiO_2 layer, bare H-(Fe)ZSM-5 and SiO_2 coated H-(Fe)ZSM-5 were studied with transmission electron microscope imaging technique. Fig. 28(a) shows the bare H-(Fe)ZSM-5 followed by our own synthesis method with template/silica ratio =

0.35. Fig. 28(b) and (c) presents the morphology of SiO_2 deposited H-(Fe)ZSM-5 which H-(Fe)ZSM-5 is taken from the exactly identical sample mentioned above. Basically, the silica layer is uniformly well-coated on the surface of H-(Fe)ZSM-5. Additionally, the thickness of silica layer is confirmed to be around 30nm which is smaller than that reported by Qian (~75nm).

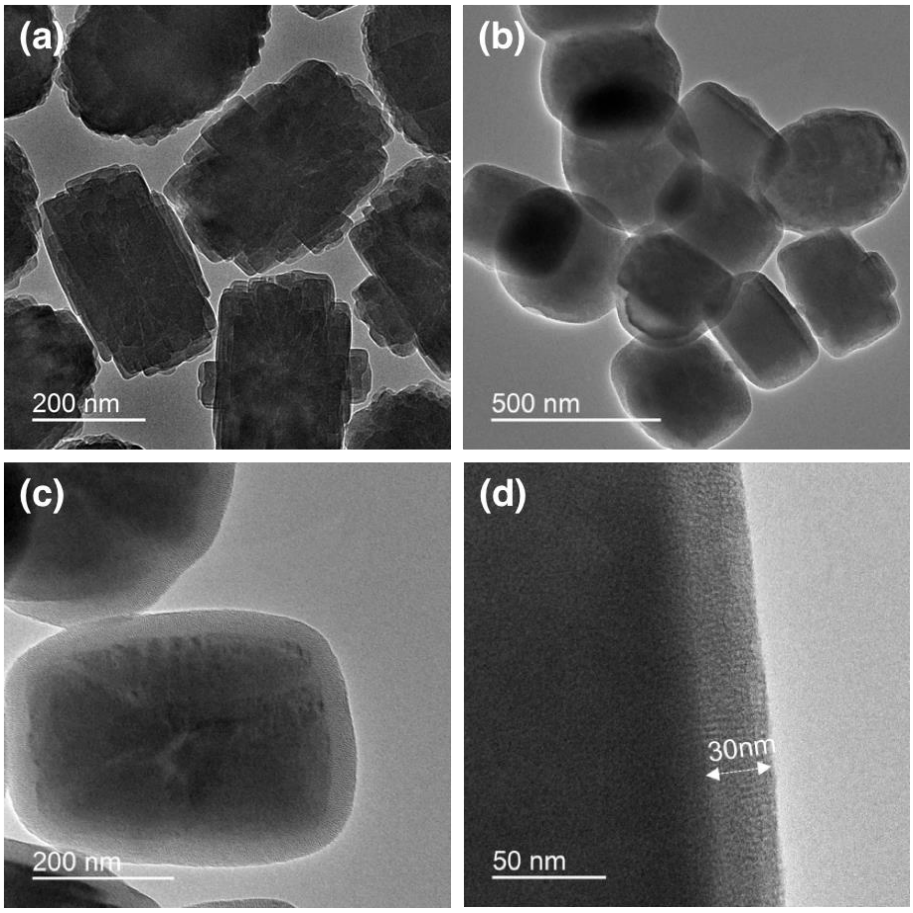

Fig. 28 Transmission electron microscope images of H-(Fe)ZSM-5 and SiO2@H-(Fe)ZSM-5: (a) H-(Fe)ZSM-5, (b) SiO2@H-(Fe)ZSM-5, (c) SiO2@H-(Fe)ZSM-5 and (d) a closer look of thickness of SiO2.

In addition to morphology analysis, porosity analysis is presented in Fig. 29. It is observed that in Fig. 29(a), N_2 adsorption/desorption is changed after coating a silica layer on H-(Fe)ZSM-5. The uptake of gas molecules for SiO_2@H-(Fe)ZSM-5 is increased at low relative pressure, and this indicates that after depositing a silica layer on ZSM-5, the amount of smaller pores is increased. Moreover, from Fig. 29(b) and (c), BJH adsorption and desorption both confirmed that a uniform mesopore distribution is formed around 3.6nm which is relatively larger than the reported value(~3nm) in ref. [53]. Both this increasing of mesopore diameter and the thinner silica layer(~30nm) may give rise to an even closer kinetic diffusion efficiency to pristine H-(Fe)ZSM-5 than the value they reported.

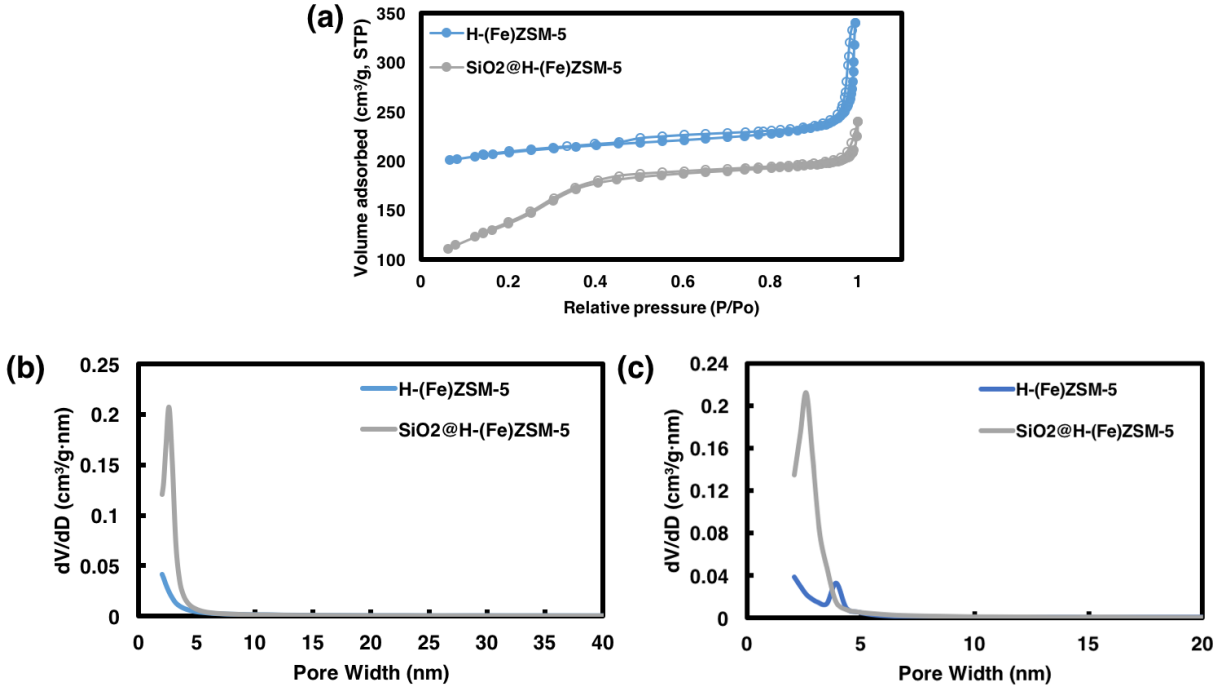

Fig. 29 Porosity analysis of of H-(Fe)ZSM-5 and SiO_2@H-(Fe)ZSM-5: (a) N_2 adsorption and desorption isotherms at 77K: enclosed symbol refers to adsorption and open symbol refers to desorption, (b) BJH mesopore size distribution taken from adsorption branch and (c) BJH mesopore distribution taken from desorption branch.

3.7.1.2 Catalytic performance

To study how the passivation of external Bronsted acid sites affects catalytic performance, SiO_2@H-(Fe)ZSM-5 was applied into DHA reaction. Fig. 30 shows the reactivity results of both pristine H-(Fe)ZSM-5 and SiO_2@H-(Fe)ZSM-5. From Fig. 30(a), methane conversion decrease dramatically after passivating the external Bronsted acid site, which is reasonable due to the loss of highly reactive surface active site. However, after passivating the external Bronsted acid site, the maximum benzene selectivity in Fig. 30(b) is remained at a similar value (~90%). It is worthwhile to mention that after reaching the maximum benzene selectivity, the deactivation rate seems to be slower, which probably indicates that passivation of external Bronsted acid site does help reduce the coke formation. However, it was expected that due to the loss of non-selective acid site, benzene selectivity can be enhanced and maintained at a higher value for a long time instead of reaching the ultimate value and dropping down immediately. The possible explanation can be diffusion limitations caused by the poor connection (mismatch) between mesoporous silica and internal microchannel. Nonetheless, the detailed explanation still need further investigations. Fig. 30 (c) and (d) show that benzene yield and benzene production follows the similar trend as benzene selectivity.

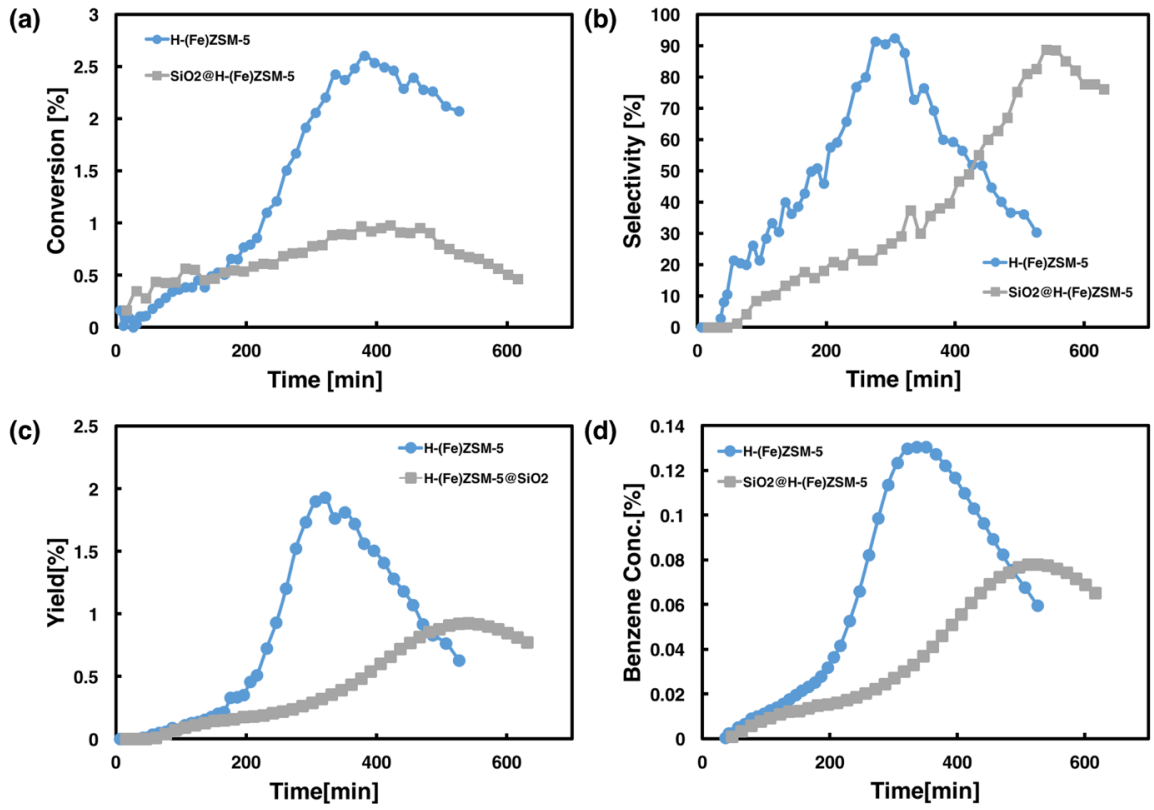

Fig. 30 Catalytic performance of SiO_2@H-(Fe)ZSM-5 and H-(Fe)ZSM-5: (a) methane conversion, (b) benzene selectivity, (c) benzene yield and (d) benzene production.

3.7.2 Conclusion

We successfully synthesized an uniformly amorphous silica layer on H-(Fe)ZSM-5 with the thickness around 30nm. Porosity analysis shows the mesoporous SiO_2 possess a narrow mesopore distribution(~3.6nm) which should have little influence on limiting molecules transportation. For reactivity, it generally follows that the passivation of external Bronsted acid site will cause decreasing of conversion and reduction of coking. However, the selectivity does not follow our hypothesis that benzene selectivity is maintained at a higher value due to the

absence of non-selective acid site on external surface. The detailed causes still need further investigations.

4.0 OUTLOOK

4.1 H-(FE)ZSM-5 CATALYST

4.1.1 Materials & Reaction condition

Y. Lai et al.[31] developed the atomically dispersed Fe modified ZSM-5 and applied into DHA reaction. Their results confirmed that highly dispersed Fe can potentially suppress the coke formation generated on Fe site, which is first proposed by Bao et al.[30], and give rise to a higher benzene selectivity comparing to other Fe modified zeolites. However, a severe coke formation still generated from the secondary reaction on Bronsted acid site. In order to further investigate the potential of this isomorphous Fe substituted ZSM-5 on DHA, we aim to study how is the catalytic performance affected by the changes in material properties.

In this study, we successfully developed a well-defined Fe modified catalyst for DHA reaction comparing to the one reported by Y. Lai et al.. Unfortunately, the best conversion reached in this study is still poor (~3%) although benzene selectivity is high (~86%). Nonetheless, it is worthwhile to mention that the space velocity of reactant used in this study is 3750 $GHSV^{-1}$ which is relatively larger than values on other literature (~1000 $GHSV^{-1}$ or below). Generally, a decreasing in space velocity of reactant, i.e. a longer residence time, should lead to a higher methane conversion but a lower selectivity which may enable this H-(Fe)ZSM-5 to have a

comparable performance comparing to Mo/HZSM-5. Apart from changing reaction condition, the increase of Fe loading can be a promising way to enhance the reactivity since the molar loading of Fe is relatively low(~0.012%) while Mo/HZSM-5 typically have at least 0.02 mole% of Mo loading. Additionally, in this study, there is no post-treatment such as alkali treatment for mesopore generation applied, which may permit the further optimization of this catalyst since the amount of mesopore formed is much lower than one generated from post-treatment.[49,62]

4.1.2 Reaction Mechanism

Apart from studying on catalyst itself, it is also worthwhile to investigate the reaction mechanism of this catalyst. Moreover, with the understanding of reaction mechanism, the direction of optimization of this material can be more straightforward. Especially, the lengthy catalyst activation period and two stages maximum reactivity are still mysteries. These questions are speculated to be the unknown transformation of Fe site inside ZSM-5. This transformation probably is related to the oxidation state of Fe site, which means that analysis instrument like X-ray photoelectron spectroscopy(XPS) and Fourier Transform Infrared Spectroscopy(FTIR) can give us an insight about what is changing during DHA reaction.

APPENDIX A

CONTROLLING CRYSTALLINITY AND PARTICLE SIZE VIA VARYING HYDROTHERMAL TIME

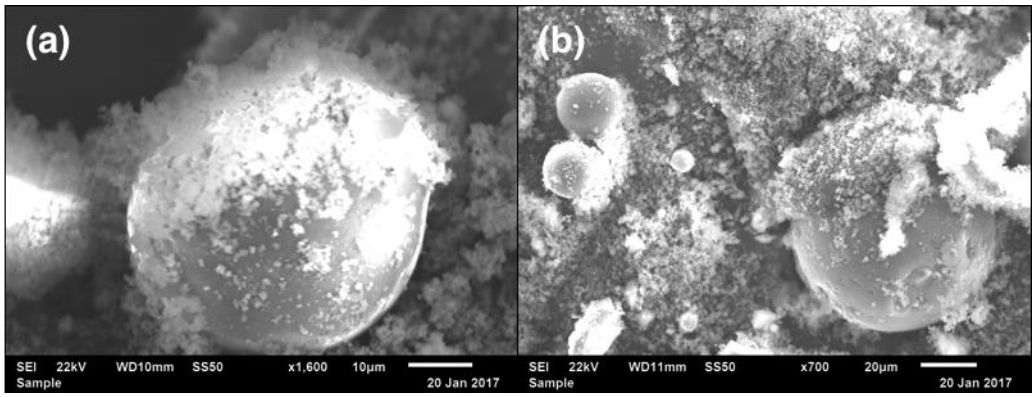

Fig. 31 Scanning microscope images of H-(Fe)ZSM-5 before hydrothermal reaction: (a) in scale of 10µm ,and (b) in scale of 20µm.

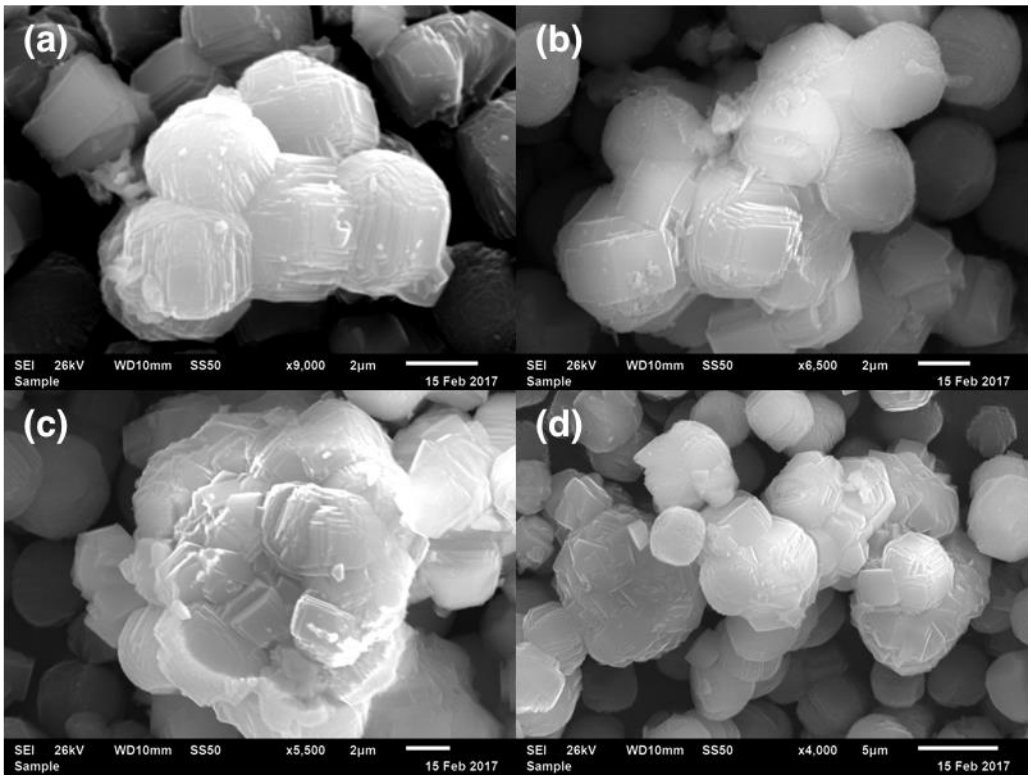

Fig. 32 Scanning microscope images of transition state of H-(Fe)ZSM-5 with different hydrothermal time: (a) 12h, (b)15h and (c)(d)18h.

CONTROLLING PARTICLE SIZE WITH FIXED MESOPOROSTIY VIA VARYING TEMPLATE/SILICA RATIO

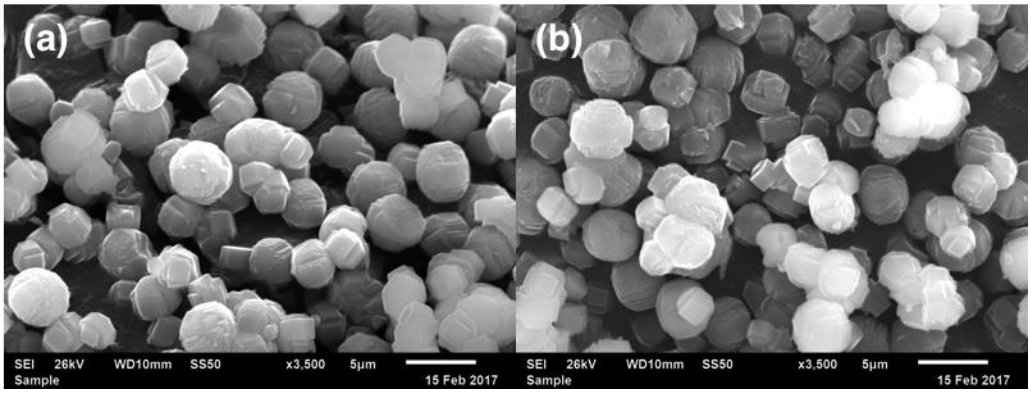

Fig. 33 Scanning microscope images H-(Fe)ZSM-5 with template/silica ratio = 0.05.

BIBLIOGRAPHY

(1) Spivey, J. J. et al., *Catalytic aromatization of methane*, Chem. Soc. Rev., 43**,** 792–803 (**2014**).

(2) Weitkamp, J., *Zeolites and catalysis*, Solid State Ionics, 131**,** 175–188 (**2000**).

(3) Cejka, J., H. van Bekkum, A. Corma & F. Schueth, *Introduction to Zeolite Molecular Sieves*, *Studies in Surface Science and Catalysis*, 168**,** (**2007**).

(4) Vermeiren, W. & J. P. Gilson, *Impact of zeolites on the petroleum and petrochemical industry*, Top. Catal., 52**,** 1131–1161 (**2009**).

(5) Horn, R. & R. Schlögl, *Methane Activation by Heterogeneous Catalysis*, Catal. Letters, 145**,** 23–39 (**2015**).

(6) Xu, Y. et al., *Methane activation without using oxidants over Mo/HZSM-5 zeolite catalysts*, Catal. Letters, 30**,** 135–149 (**1994**).

(7) Weckhuysen, B. M., D. Wang, M. P. Rosynek & J. H. Lunsford, *Conversion of Methane to Benzene over Transition Metal Ion ZSM-5 Zeolites: II. Catalyst Characterization by X-Ray Photoelectron Spectroscopy*, J. Catal., 175**,** 347–351 (**1998**).

(8) Weckhuysen, B. M., D. Wang, M. P. Rosynek & J. H. Lunsford, *Conversion of Methane to Benzene over Transition Metal Ion ZSM-5 Zeolites: I. Catalytic Characterization*, J. Catal., 175**,** 347–351 (**1998**).

(9) Ohnishi, R. et al., *Catalytic Dehydrocondensation of Methane with CO and CO2 toward Benzene and Naphthalene on Mo/HZSM-5 and Fe/Co-Modified Mo/HZSM-5*, J. Catal., 182**,** 92–103 (**1999**).

(10) Behrsing, T., H. Jaeger & J. V. Sanders, *Coke deposits on H-ZSM-5 zeolite*, Appl. Catal., 54**,** 289–302 (**1989**).

(11) Forzatti, P. & L. Lietti, *Catalyst deactivation*, Catal. Today, 52**,** 165–181 (**1999**).

(12) Chen, L., *Dehydro-oligomerization of Methane to Ethylene and Aromatics over Molybdenum/HZSM-5 Catalyst*, *Journal of Catalysis*, 157**,** 190–200 (**1995**).

(13) Bai, J. et al., *Comparison of 6Mo/MCM-22 and 6Mo/ZSM-5 in the MDA process*, React. Kinet. Catal. Lett., 82**,** 279–286 (**2004**).

(14) Schüth, F. & W. Schmidt, *Microporous and mesoporous materials*, Adv. Mater., 14**,** 629–638 (**2002**).

(15) Chu, N. et al., *An unusual hierarchical ZSM-5 microsphere with good catalytic performance in methane dehydroaromatization*, Microporous Mesoporous Mater., 118**,** 169–175 (**2009**).

(16) Triantafillidis, C. S., A. G. Vlessidis & N. P. Evmiridis, *Effect of the degree and type of the dealumination method on the structural, compositional and acidic characteristics of H-ZSM-5 zeolites*, Ind. Eng. Chem. Res., 39**,** 307–319 (**2000**).

(17) Groen, J. C. et al., *Direct demonstration of enhanced diffusion in mesoporous ZSM-5 zeolite obtained via controlled desilication*, J. Am. Chem. Soc., 129**,** 355–360 (**2007**).

(18) Groen, J. C. et al., *Creation of hollow zeolite architectures by controlled desilication of A1-zoned ZSM-5 crystals*, J. Am. Chem. Soc., 127**,** 10792–10793 (**2005**).

(19) Pérez-Ramírez, J. et al., *Hierarchical zeolites: Enhanced Utilisation of Microporous Crystals in Catalysis by Advances in Materials Design.*, Chem. Soc. Rev., 37**,** 2530–2542 (**2008**).

(20) Jacobsen, C. J. H. et al., *Mesoporous zeolite single crystals*, J. Am. Chem. Soc., 122**,** 7116–7117 (**2000**).

(21) Schmidt, I. et al., *Carbon nanotube templated growth of mesoporous zeolite single crystals*, Chem. Mater., 13**,** 4416–4418 (**2001**).

(22) Larsen, S. C., *Nanocrystalline zeolites and zeolite structures: Synthesis, characterization, and applications*, J. Phys. Chem. C, 111**,** 18464–18474 (**2007**).

(23) Song, W. et al., *Size-dependent properties of nanocrystalline silicalite synthesized with systematically varied crystal sizes*, Langmuir, 20**,** 4696–4702 (**2004**).

(24) Zhang, W. P. et al., *Methane dehydro-aromatization over Mo/HZSM-5 in the absence of oxygen: A multinuclear solid-state NMR study of the interaction between supported Mo species and HZSM-5 zeolite with different crystal sizes*, J. Catal., 188**,** 393–402 (**1999**).

(25) Cui, Y. et al., *The effect of zeolite particle size on the activity of Mo/HZSM-5 in non-oxidative methane dehydroaromatization*, Appl. Catal. A Gen., 393**,** 348–358 (**2011**).

(26) Wang, L. et al., *Dehydrogenation and aromatization of methane under non-oxidizing conditions*, Catal. Letters, 21**,** 35–41 (**1993**).

(27) Xu, Y. & L. Lin, *Recent advances in methane dehydro-aromatization over transition metal ion-modified zeolite catalysts under non-oxidative conditions*, Appl. Catal. A Gen., 188**,** 53–67 (**1999**).

(28) Wang, L., R. Ohnishi & M. Ichikawa, *Selective Dehydroaromatization of Methane toward Benzene on Re/HZSM-5 Catalysts and Effects of CO/CO2 Addition*, J. Catal., 190**,** 276–283 (**2000**).

(29) Guczi, L. & I. Kiricsi, *Zeolite Supported Mono- and Bimetallic Systems: Structure and Performance as CO Hydrogenation Catalysts*, Appl. Catal. A Gen., 186**,** 375–394 (**1999**).

(30) Guo, X. et al., *Direct, nonoxidative conversion of methane to ethylene, aromatics, and hydrogen.*, Science, 344**,** 616–9 (**2014**).

(31) Lai, Y. & G. Veser, *The Nature of the Selective Species in Fe-HZSM-5 for Non-Oxidative Methane Dehydroaromatization*, Catal. Sci. Technol., 6**,** 5440–5452 (**2016**).

(32) Awala, H. et al., *Template-free nanosized faujasite-type zeolites.*, Nat. Mater., 14**,** 447–51 (**2015**).

(33) Pérez-Ramírez, J. et al., *Physicochemical Characterization of Isomorphously Substituted FeZSM-5 during Activation*, J. Catal., 207**,** 113–126 (**2002**).

(34) American Society for Testing and Material, *Standard Test Method for Determination of Relative Crystallinity of Zeolite ZSM-5 by X-Ray Diffraction*, 1**,** (**2011**).

(35) Grieken, R. Van, J. L. Sotelo, J. M. Menendez & J. A. Melero, *Anomalous crystallization mechanism in the synthesis of nanocrystalline ZSM-5*, Microporous Mesoporous Mater., 39**,** 135–147 (**2000**).

(36) Tartaj, P. et al., *The preparation of magnetic nanoparticles for applications in biomedicine*, J. Phys. D. Appl. Phys., 36**,** 182–197 (**2003**).

(37) LaMer, V. K. & R. H. Dinegar, *Theory, production and mechanism of formation of monodispersed hydrosols*, J. Am. Chem. …, 72**,** 4847–4854 (**1950**).

(38) Matsoukas, T. & E. Gulari, *Self-sharpening distributions revisited-polydispersity in growth by monomer addition*, J. Colloid Interface Sci., 145**,** 557–562 (**1991**).

(39) Li, X., F. Zhang & D. Zhao, *Lab on upconversion nanoparticles: optical properties and applications engineering via designed nanostructure*, Chem. Soc. Rev., 44**,** 1346–1378 (**2015**).

(40) Murray, C. B., C. R. Kagan & M. G. Bawendi, *Synthesis and characterization of monodisperse nanocrystals and close-packed nanocrystal assemblies*, Annu. Rev. Mater. Sci., 30**,** 545–610 (**2000**).

(41) Crea, F., A. Nastro, J. B. Nagy & R. Aiello, *Synthesis of silicalite 1 from systems with different TPABr/SiO2 ratios*, Zeolites, 8**,** 262–267 (**1988**).

(42) Ding, L. & Y. Zheng, *Effect of template concentration and gel dilution on crystallization and particle size of zeolite beta in the absence of alkali cations*, Microporous Mesoporous Mater., 103**,** 94–101 (**2007**).

(43) Cundy, C. S., B. M. Lowe & D. M. Sinclair, *Crystallisation of zeolitic molecular sieves: direct measurements of the growth behaviour of single crystals as a function of synthesis conditions*, Faraday Discuss., 95**,** 235 (**1993**).

(44) Persson, A. E., B. J. Schoeman, J. Sterte & J.-E. Otterstedt, *The synthesis of discrete colloidal particles of TPA-silicalite-1*, Zeolites, 14**,** 557–567 (**1994**).

(45) Fouad, O. A., R. M. Mohamed, M. S. Hassan & I. A. Ibrahim, *Effect of template type and template/silica mole ratio on the crystallinity of synthesized nanosized ZSM-5*, Catal. Today, 116**,** 82–87 (**2006**).

(46) Petushkov, A., S. Yoon & S. C. Larsen, *Synthesis of hierarchical nanocrystalline ZSM-5 with controlled particle size and mesoporosity*, Microporous Mesoporous Mater., 137**,** 92–100 (**2011**).

(47) Thommes, M. et al., *Adsorption hysteresis of nitrogen and argon in pore networks and characterization of novel micro- and mesoporous silicas*, Langmuir, 22**,** 756–764 (**2006**).

(48) Groen, J. C., L. A. A. Peffer & J. Pérez-Ramírez, *Pore size determination in modified micro- and mesoporous materials. Pitfalls and limitations in gas adsorption data analysis*, Microporous Mesoporous Mater., 60**,** 1–17 (**2003**).

(49) Groen, J. C., L. A. A. Peffer, J. A. Moulijn & J. Pérez-Ramírez, *Mesoporosity development in ZSM-5 zeolite upon optimized desilication conditions in alkaline medium*, Colloids Surfaces A Physicochem. Eng. Asp., 241**,** 53–58 (**2004**).

(50) Itani, L. et al., *Investigation of the physicochemical changes preceding zeolite nucleation in a sodium-rich aluminosilicate gel*, J. Am. Chem. Soc., 131**,** 10127–10139 (**2009**).

(51) Persson, A. E., B. J. Schoeman, J. Sterte & J. E. Otterstedt, *Synthesis of stable suspensions of discrete colloidal zeolite (Na, TPA)ZSM-5 crystals*, Zeolites, 15**,** 611–619 (**1995**).

(52) Yan, Y., M. E. Davis & G. R. Gavalas, *Preparation of zeolite ZSM-5 membranes by in-situ crystallization*, Ind. Eng. Chem. Res., 34**,** 1652–1661 (**1995**).

(53) Mostowicz, R. & J. M. Berak, *Factors Influencing the Crystal Morphology of ZSM-5 Type Zeolites*, *Studies in Surface Science and Catalysis*, 24**,** (Elsevier Science Publishers B.V., **1985**).

(54) Koegler, J. H., H. van Bekkum & J. C. Jansen, *Growth model of oriented crystals of zeolite Si-ZSM-5*, Zeolites, 19**,** 262–269 (**1997**).

(55) Gabelica, Z., N. Blom & E. G. Derouane, *Synthesis and Characterization of ZSM-5 Type Zeolite: III. A critical evaulation of the role of alkali and ammonium cations*, Appl. Catal., 5**,** 227–248 (**1983**).

(56) Ding, W., G. D. Meitzner & E. Iglesia, *The Effects of Silanation of External Acid Sites on the Structure and Catalytic Behavior of Mo/H–ZSM5*, J. Catal., 206**,** 14–22 (**2002**).

(57) Bhat, Y. S., J. Das, K. V. Rao & A. B. Halgeri, *Inactivation of External Surface of ZSM-5: Zeolite Morphology, Crystal Size, and Catalytic Activity*, J. Catal., 159**,** 368–374 (**1996**).

(58) Wang, I., C.-L. Ay, B.-J. Lee & M.-H. Chen, *Para-selectivity of dialkylbenzenes over modified HZSM-5 by vapour phase deposition of silica*, Appl. Catal., 54**,** 257–266 (**1989**).

(59) Lv, Y., X. Qian, B. Tu & D. Zhao, *Generalized synthesis of core-shell structured nano-zeolite@ordered mesoporous silica composites*, Catal. Today, 204**,** 2–7 (**2013**).

(60) Qian, X. F. et al., *Exploring meso-/microporous composite molecular sieves with core-shell structures*, Chem. - A Eur. J., 18**,** 931–939 (**2012**).

(61) Prokešová, P. et al., *Catalytic activity of micro/mesoporous composites in toluene alkylation with propylene*, Appl. Catal. A Gen., 281**,** 85–91 (**2005**).

(62) Ogura, M. et al., *Alkali-treatment technique - New method for modification of structural and acid-catalytic properties of ZSM-5 zeolites*, Appl. Catal. A Gen., 219**,** 33–43 (**2001**).